

Application of fuzzy *c*-means clustering for analysis of chemical ionization mass spectra: insights into the gas-phase chemistry of NO₃-initiated oxidation of isoprene

Rongrong Wu¹, Sören R. Zorn¹, Sungah Kang¹, Astrid Kiendler-Scharr^{1†}, Andreas Wahner¹
5 and Thomas F. Mentel^{1*}

¹Institute of Energy and Climate Research, Troposphere (IEK-8), Forschungszentrum Jülich GmbH, 52428 Jülich, Germany

† Deceased February-06th, 2023

10 *Correspondence to: Thomas F. Mentel (t.mentel@fz-juelich.de)

Abstract

Oxidation of volatile organic compounds (VOCs) can lead to the formation of secondary
15 organic aerosol, a significant component of atmospheric fine particles, which can affect air
quality, human health, and climate change. However, current understanding of the formation
mechanism of SOA is still incomplete, which is not only due to the complexity of the
chemistry, but also relates to analytical challenges in SOA precursor detection and
quantification. Recent instrumental advances, especially the developments of high-resolution
20 time-of-flight chemical ionization mass spectrometry (CIMS), greatly ~~enhanced the
capability improved both detection and quantification of to detect~~ low- and extremely low-
volatility organic molecules (L/ELVOCs), which largely facilitated the investigation of
SOA formation pathways. Although detection and characterization of low volatility vapors
largely improved our understanding of SOA formation However, analyzing and interpreting
25 complex mass spectrometric data remains a challenging task. This necessitates the use of
dimension-reduction techniques to simplify mass spectrometric data with the purpose of
extracting chemical and kinetic information of the investigated system. Here we present an
approach ~~by using to apply~~ fuzzy *c*-means clustering (FCM) to analyze CIMS data from a
chamber experiments, aiming to investigate the gas-phase chemistry of nitrate radical
30 initiated oxidation of isoprene.

The performance of FCM was evaluated and validated. By applying FCM ~~to
measurements,~~ various oxidation products were classified into different groups ~~according~~

35 ~~te~~based on their chemical and kinetic properties, and the common patterns of their time series were identified, which gave insights into the chemistry of the investigated system investigated. The chemical properties of clusters are ~~eharacterized~~described by elemental ratios and average carbon oxidation state, and the kinetic behaviors are parameterized with generation number and effective rate coefficient (describing the average reactivity of a species) by using the gamma kinetic parameterization model. In addition, the fuzziness of FCM algorithm provides a possibility to separate isomers or different chemical processes
40 species are involved in, which could be useful for mechanism development. Overall FCM is a well applicable technique to simplify complex mass spectrometric data, and the chemical and kinetic properties derived from clustering can be utilized to understand the reaction system of interest.

1. Introduction

45 Volatile organic compounds (VOCs) in the atmosphere are oxidized by reactions with
hydroxyl radicals (OH), ozone (O₃), nitrate radicals (NO₃), or Cl atoms, ~~leading to the~~
~~formation and converted to of~~ condensable vapors such as low- and extremely low-volatility
organic compounds (LVOCs/ ELVOCs) that subsequently ~~can~~ condense onto existing
50 particles or even form new particles, and thereby form secondary organic aerosol (SOA)
(Donahue et al., 2012; Hallquist et al., 2009; Ziemann and Atkinson, 2012). ~~Secondary~~
~~organic aerosol~~ SOA comprises a major fraction of the atmospheric submicron particulate
matter and can have an adverse impact on air quality, human health, and climate (Hallquist et
al., 2009; Jimenez et al., 2009; Pöschl, 2005; Spracklen et al., 2011; Zhang et al., 2007).
Despite extensive studies on characterization of the products and mechanisms involved in
55 VOC oxidation and SOA formation, how VOCs contribute to SOA formation is not yet fully
understood. This is not only hampered by the complexity of the chemistry itself, but also by
the remaining analytical challenges in detection of organic precursors with low volatility
(Bianchi et al., 2019; Shrivastava et al., 2017).

Recent instrumental developments, especially the ~~propagation availability~~ of high-
60 resolution time-of-flight chemical ionization mass spectrometry (CIMS) ~~in atmospheric~~
~~research~~, made the direct detection of low-volatility vapors possible (Ehn et al., 2012; Ehn et
al., 2014; Jokinen et al., 2015). Benefitting from this, it has been discovered that the highly
oxygenated organic molecules (HOM), which are formed through a rapid gas-phase process
called autooxidation and generally have very low volatilities, significantly contribute to SOA
65 and even new particle formation (Crouse et al., 2013; Ehn et al., 2012; Ehn et al., 2014;
Kirkby et al., 2016; Praske et al., 2018).

While advanced mass spectrometers greatly enhance our capability to ~~detect and~~
~~quantify HOM and facilitate the investigation of HOM formation mechanism, investigate the~~
~~chemical composition and evolution of HOM,~~ the highly complex mass spectrometric data,
70 ~~consisting which consists~~ of hundreds to thousands of variables (i.e., detected ions) over
thousands of points in time, makes the data processing and interpretation challenging. In
addition, ~~the molecular structure information of detected ions can only be extrapolated from~~
~~their chemical composition, notwithstanding~~ the mass spectrometers are unable to detect
~~structures of molecules despite the~~ modern ~~apparatus instruments of with~~ high resolution (e.g.,
75 over 10,000 m/Δm) (Breitenlechner et al., 2017; Krechmer et al., 2018), which significantly
hinders the understanding of the involved chemical processes. Furthermore, it is difficult to

refine and extract kinetic and mechanistic information directly from the mass spectrometric data.

80 To reduce ~~this the~~ complexity of data analysis, dimension-reduction techniques are necessary, which compress ~~the information~~ various variables in a dataset into a few to a dozen of factors ~~or~~ clusters based on the underlying correlation/ similarity ~~physical or chemical properties~~ of the different variables, e.g., in terms of their sources or physicochemical properties, ~~and thus while retain the major chemical and kinetic information simplify the chemistry~~ of investigated systems, and thus make the data analysis easier and more effective
85 (Äijälä et al., 2017; Buchholz et al., ~~2019~~2020; Koss et al., 2020; Yan et al., 2016; Zhang et al., 2019).

Factorization is one of the major ~~data~~ dimension-reduction techniques, within which positive matrix factorization (PMF) (Paatero, 1997; Paatero and Tapper, 1994) is the ~~best-known~~ most commonly used approach in atmospheric science, especially for ambient
90 measurements of particulate matter by aerosol mass spectrometer (Canonaco et al., 2013; Lanz et al., 2007; Lanz et al., 2008; Zhang et al., 2005; Zhang et al., 2011), as well as for VOC measurements in both field and laboratory studies (Brown et al., 2007; Lanz et al., 2009; Li et al., 2021; Rosati et al., 2019; Vlasenko et al., 2009; Yuan et al., 2012). Principal component analysis (PCA) (Wold et al., 1987) is also a frequently used multivariate factor
95 analysis technique for deconvolution and interpretation of gas-~~phase~~ and particle-phase composition data (Sofowote et al., 2008; Wyche et al., 2015; Zhang et al., 2005). Additionally, non-negative matrix factorization (NMF), which is very similar to the PMF approach, has been widely used in interdisciplinary fields (Devarajan, 2008; Fu et al., 2019; Lee and Seung, 1999), as well as in atmospheric science (Chen et al., 2013; Karl et al., 2018;
100 Malley et al., 2014; Song et al., 2021). Despite the similarities ~~of in~~ mathematical formulation and constraints to PMF, the NMF algorithm does not ~~require~~ need an error matrix as input, ~~largely reducing the uncertainties that might be introduced by inappropriate error estimation methods (Buchholz et al., 2019)~~ This eliminates the potential impact of error estimation on outcomes and makes it more user-friendly.

105 In addition to factorization methods, ~~recently an~~ increasing number of recent studies have employed ~~adopted~~ clustering techniques to mass spectra data (Äijälä et al., 2017; Koss et al., 2020; Li et al., 2020; Priestley et al., 2021). For example, Äijälä et al. (2017) combined a clustering algorithm, *k*-means ++, with PMF to classify and characterize the organic component of air pollution plumes detected by AMS. Li et al. (2020) developed a clustering
110 algorithm named noise-sorted scanning clustering, based on the traditional density-based

special clustering of applications combined with a noise algorithm, and thereafter applied this method to distinguish different types of thermal properties of ~~different-variousnt~~ biogenic SOA. Koss et al. (2020) compared the performance of hierarchical clustering analysis (HCA) with PMF and gamma kinetics parameterization ~~for-in~~ analyzing complex mass spectrometric data. Their results demonstrate the ~~ability-feasibility~~ of HCA to identify major types of ions and patterns of time behavior and ~~to~~ draw out bulk chemical properties of the system that can be useful for modeling. In addition, in a recent work ~~by~~ Priestley et al. (2021), ~~applied~~ HCA ~~techniques-was-applied~~ to infer CHON functionality of products formed from benzene oxidation.

In this work, we choose the fuzzy *c*-means clustering algorithm (FCM) as the major technique to analyze CIMS data collected from a chamber experiment, aiming to investigate the gas-phase chemistry of the isoprene-NO₃ oxidation system. ~~Isoprene is the most abundant BVOC on earth, and is highly reactive in the atmosphere, which is an important precursor of O₃ and SOA and thus imposes detrimental effects on climate and health (Carlton et al., 2009; Surratt et al., 2019). The reaction of isoprene with NO₃ is an important source of SOA, but its gas-phase reaction mechanism, especially the multi-generation chemistry and the contribution of the corresponding oxidation products to SOA formation remain ambiguous so far (Carlton et al., 2009; Fry et al., 2018; Ng et al., 2008; Rollins et al., 2009; Wu et al., 2021).~~ Fuzzy *c*-means clustering is the most widely used fuzzy clustering algorithm and is adopted in this study considering the following ~~two-three~~ aspects. Firstly, FCM allows variables to be affiliated with ~~more-than-one~~ multiple clusters, ~~as-similar to factorization methods like PMF, NMF, and PCAPMF does,-, whereas~~ Conversely, hard clustering methods, ~~like-such as~~ the most popular *k*-means clustering, ~~foree~~ assigns each variable ~~exclusively~~ into one cluster ~~exclusively~~. In atmospheric chemistry, one compound can originate from several different sources, or a species detected may consist of isomers produced from different chemical processes. Therefore, ~~from this perspective,~~ assigning a variable into multiple clusters with a quantified membership degree is more rational ~~in this ease~~ than assigning variables to mutually exclusive clusters. Secondly, FCM ~~is more user-friendly since~~ only ~~needs-athe~~ data matrix ~~is needed~~ as input, whereas ~~additional information is required~~ for ~~some~~-factor analysis methods ~~additional information is required~~, such as the error matrix needed in PMF_{*n*}, ~~which is usually estimated by user-defined error estimation schemes and could result in perceptibly different outcomes accordingly (Buchholz et al., 2019; Paatero et al., 2014; Paatero and Tapper, 1994; Ulbrich et al., 2009)~~ Furthermore, receptor models like PMF assume that the factor profiles remain constant over time and that the chemical species do not react with each

hat formatiert: Tiefgestellt

hat formatiert: Tiefgestellt

145 ~~other during the sampling period (Chen et al., 2011; Reff et al., 2007; Xie et al., 2022), which is not the case for chamber measurements.~~

By using FCM, variables with similar time behaviors will be grouped into the same cluster, and the centroid of ~~this-the~~ cluster (cluster center) can be used as a surrogate of these variables. Therefore, the numerous species detected in a chemical system can be ~~simplified~~
150 ~~compressed and characterized by~~to a much smaller number of clusters, each of which represents a typical chemical process/~~source~~ with unique ~~kinetic-time~~ behavior. ~~By analyzing these cluster centers instead of the whole data set, one can obtain the chemical and kinetic properties of the investigated system in a much easier way.~~ The significant reduction of the complexity of ~~the chemical system data analysis~~ and the chemical and kinetic information
155 derived from this method can help to better understand the chemical system of interest (Koss et al., 2020). In addition, ~~to evaluate its performance,~~ we applied FCM to a synthetic dataset derived from a box model with explicit mechanism ~~to evaluate the performance of FCM clustering.~~ By exemplifying the functionality of such a clustering method in analyzing CIMS data, we propose that FCM is a useful method that offers a new ~~way-approach~~ to analyze
160 mass spectrometric data and ~~to~~ derives useful information on chemical and kinetic properties of products that can help decipher the underlying reaction mechanism.

2. Methods

2.1 Data collection and processing

The experimental data used in this work were collected in the atmospheric simulation
165 chamber SAPHIR at the Forschungszentrum Jülich, Germany, during the ISOPNO₃ campaign in 2018. The SAPHIR chamber is a double-walled Teflon (PEP) cylinder with an approximate volume of 270 m³ (5m in diameter, 20m in length). It is fixed by an aluminum frame with movable shutters that can be opened or closed to simulate daytime or nighttime chemistry. Trace gases in the chamber can be well mixed within 2 minutes with the help of
170 two continuously operated fans. During an experiment, the chamber is filled with synthetic air and kept slightly over pressured (~ 35 Pa) to prevent permeation of outside air into the chamber. Due to small leakages and instrument sampling consumption, there is a replenishing flow into the chamber, which leads to a dilution rate of 4% – 7% h⁻¹. More details about the chamber setup and its performance can be found elsewhere (Rohrer et al., 2005).

175 The experiment selected here was conducted to characterize the gas-phase chemistry of
NO₃-initiated oxidation of isoprene. ~~O₃ and NO₂ were added in sequence to produce~~
~~NO₃. Nitrate radicals were produced in situ by the reaction of NO₂ with O₃,~~ followed by the
addition of ~10 ppbv of isoprene to initiate the reaction. The injections ~~was~~ were repeated
180 four times (only NO₂ and O₃ were added ~~during in~~ the last injection) to build up products and
to facilitate later-generation oxidation. The mixing ratios of O₃ and NO₂ in the chamber were
approximately 100 and 25 ppbv, respectively, after the first injection, ~~but this was not~~
~~uniform every time~~, as shown in Fig. S1. Detailed description of the experimental procedure
can be found elsewhere (Wu et al., 2021).

185 During the campaign, a comprehensive set of instruments was deployed ~~for the~~
~~measurements to measure~~ of radicals and closed-shell products in both gas- and particle-
phase, as described by Wu et al. (2021). In this work, however, we focus on the
measurements acquired by a high-resolution time-of-flight chemical ionization mass
spectrometer (Aerodyne Research Inc.) using Br⁻ as reagent ion, which detected the HO₂
190 radical and the gas-phase products generated by the reaction of isoprene and NO₃. The mass
spectrometer was operated in “V” mode with a mass resolution of 3000 – 4000 ($m/\Delta m$). A
customized inlet was designed to connect the CIMS directly to the chamber to reduce losses
of the HO₂ radical and HOM in the sampling line (Albrecht et al., 2019). More information
about settings and performance of the instrument can be found in our previous study (Wu et
al., 2021).

195 The raw mass spectrometric data were processed using the Tofware toolkit (v. 2.5.11,
Tofwerk AG/ Aerodyne Research Inc.) in Igor Pro (v.7.0.8, WaveMetrics) following the
routines described by Stark et al. (2015). High-resolution peak fitting was conducted in the
mass range of m/z 60 – 600 to identify the chemical composition of detected ions. For high-
resolution peak assignment, we fitted the observed peaks using predefined instrument
200 functions (including peak shape, peak width as a function of m/z , and baseline). If necessary,
contributions of more than one component were considered for the fit, in order to reduce the
residuals of the fitting. Once the peak numbers and peak positions were fixed, the chemical
formula (consisting of C, H, O, and N atoms) of each peak was assigned manually by
selecting from a formula list generated by the software. During the peak fitting, isotopes were
205 constrained, and only plausible formulas with relative m/z deviations smaller than 10 ppm
were considered. In addition, only molecule formulas with a time behavior commensurable
with expectations for the specific chemical system were assigned (Pullinen et al., 2020). For

hat formatiert: Tiefgestellt

hat formatiert: Tiefgestellt

hat formatiert: Tiefgestellt

example, it is illogical if large amounts of organonitrates are observed under low NO_x conditions.

210 Overall, ~~more than 500 peaks around 160 ions~~ were ~~detected above the background in the mass spectra obtained~~ identified by the Br-CIMS. The background signal of each peak-ion was determined from measurements prior to precursor injection and was subtracted from the signal measured in the chamber. These ~~peaks-ions~~ consist of ~~ions-species~~ related to real isoprene oxidation products, as well as other signals related to the ion source, internal
215 standard, and interferences from chamber and tubing.

The product ions are those produced by isoprene oxidation, and they should have ~~pronounced-visible~~ changes (either increase or decrease) when the chemistry is initiated or modified. ~~Therefore, a~~ simple way to ~~screen-select~~
220 identify the product ions from other chemically irrelevant signals is to examine the time evolution of each ion. By comparing the signals before and after each injection, we can easily distinguish the product ions from others.

~~Among all the identified ions, a total of 91 ions were recognized as product signals. However, this cannot exclude variabilities unrelated to oxidation chemistry during the experiment itself. Therefore, high-resolution analysis was conducted in the mass range of m/z 60–600 to identify the chemical composition of detected ions. For high-resolution peak assignment, we fitted the observed peak using predefined instrument functions (including peak shape, peak width as a function of m/z , and baseline). If necessary, contributions of more than one component were considered for the fit to reduce the residuals of the fitting. Once the peak numbers and peak positions were fixed, the chemical formula (consisting of C, H, O, and N atoms) of each peak was assigned manually by selecting from a formula list generated by the software. During the peak fitting isotopes were constrained, and only formulas within an accuracy tolerance of 10 ppm and with reasonable chemical meanings were considered. In addition, only molecule formulas with a time behavior commensurable with expectations for the specific chemical system were assigned (Pullinen et al., 2020). For example, it is illogical if large amounts of organonitrates are observed under low NO_x conditions. Since we intend to investigate the underlying chemical relationships of different products through their time behavior, not the absolute concentration, normalized (to the sum of total ion counts) signals were ~~finally~~
225 used for further analysis. Calibration procedures are described in more detail elsewhere (Wu et al., 2021).~~

230

235

In addition to abovementioned chamber data, we use a synthetic dataset from a box
240 model with the default gas-phase reaction schemes of isoprene-NO₃ taken from the Master Chemical Mechanism (MCM) version 3.3.1 (Jenkin et al., 2015). For the modelling,

temperature, relative humidity, and dilution rate were constrained by using measured data. The initial concentrations of O₃, NO₂ and isoprene were added into the model according to the experimental schedule. Overall, the modelled concentrations of O₃, NO₂, NO₃ and isoprene match the measurements well (Fig. S2). ~~Here we only use t~~The synthetic data was used to learn about the principal behaviors of time series (of products) in a complex chemical systems ~~using with~~ an established complex mechanism. Detailed description of isoprene-NO₃ chemistry and evaluation of the model performance are outside the scope of this work. ~~An recent~~ updated mechanism for isoprene ~~+oxidation by~~ NO₃ has been published recently ~~by can be found in~~ Carlsson et al. (2022).

2.2 Fuzzy *c*-means clustering (FCM)

Clustering is one of the major dimension-reduction techniques besides factorization, which groups a set of objects into a certain number of clusters according to their (dis)similarities, ~~(which are generally measured by a distance metric)~~, such that objects within each cluster are much closer to each other than to those pertaining to other clusters (Hastie et al., 2009). The notion of a fuzzy set, ~~was first~~ proposed by Zadeh (1965), ~~which gave~~ gives an idea how to deal with data with indistinct boundaries of clusters. Based on this concept, Bezdek et al. (1984) developed the fuzzy *c*-means clustering algorithm. In contrast to the hard clustering counterparts ~~such as like~~ *k*-means and *k*-medoids clustering, FCM allows each object to belong to multiple clusters with the membership degree measured by a value varying from 0 to 1 (Bezdek et al., 1984). Consequently, fuzzy clustering can better deal with non-discrete data, and thus is adopted here to analyze ~~our~~ CIMS data ~~for the example of~~ obtained from isoprene-NO₃ oxidation.

Fuzzy *c*-means clustering is one of the best-known fuzzy clustering algorithms by virtue of its simplicity, quick convergence, and wide applicability (Ghosh and Dubey, 2013; Ren et al., 2016; Yang, 1993;). It is a distance-based cluster assignment method, and its working principle is very similar to that of the *k*-means algorithm. FCM is conducted through an iterative process which attempts to group all objects within a dataset into a predefined number of clusters (*c*) with a degree of membership, and meanwhile minimize the sum of squared distance between the member objects and the cluster centroids ~~of each cluster~~, as defined in Eq. 1:

$$J_m(U, V) = \sum_{i=1}^c \sum_{j=1}^n u_{ij}^m d_{ij}^2 \quad (1)$$

275 where x_j is the object j in the dataset, u_{ij} is the membership degree of x_j to the i^{th} cluster, which is enforced to satisfy $u_{ij} \in [0, 1]$ and $\sum_{i=1}^c u_{ij} = 1$, d_{ij} denotes the distance between object x_j and the i^{th} cluster center v_i , and m is the fuzzifier ($m \in [1, \infty)$) that controls the fuzziness level of clustering.

Starting with an initial fuzzy partition matrix (U^0), either provided or randomly produced, the cluster centers (V) are calculated by

$$v_i = \frac{\sum_{j=1}^n u_{ij}^m \cdot x_j}{\sum_{j=1}^n u_{ij}^m} \quad (2)$$

280 for all j ($1 \leq i \leq c$) and afterwards the membership degrees of each object are updated by

$$u_{ij} = \left\{ \sum_{k=1}^c \left(\frac{d_{ij}}{d_{kj}} \right)^{\frac{2}{m-1}} \right\}^{-1} \quad (3)$$

285 where x_j represents the j^{th} object in the dataset, u_{ij} is the membership degree of x_j to the i^{th} cluster, which is enforced to satisfy $u_{ij} \in [0, 1]$ and $\sum_{i=1}^c u_{ij} = 1$, $d_{ij} = \|x_j - v_i\|$ denotes the distance between object x_j and the i^{th} cluster center v_i , and m is the fuzzifier ($m \in [1, \infty)$) that controls the fuzziness level of clustering.

290 The clustering procedure of FCM is executed through an iterative strategy to minimize the objective function $J_m(U, V)$. By initializing the fuzzy partition matrix U randomly, one can compute the cluster centers (V) according to Eq. 2 with the constraint of the sum of the membership degrees of an object to all clusters being unity. In the consecutive iteration, new membership degrees are calculated following Eq. 3. The calculation algorithm proceeds by repeating above process, and every iteration generates two new sets of V and U . The iteration ends when the algorithm converges (no significant change with further iteration, namely $\|U^{(t+1)} - U^{(t)}\| = \max_{i,j} \{ |u_{ij}^{(t+1)} - u_{ij}^t| \} < \varepsilon$), or the predefined maximum number of iterations is reached. In this study, the FCM algorithm was implemented using the open-source scikit-fuzzy (v 0.4.2) package (<https://pypi.org/project/scikit-fuzzy/>) in Python.

2.3 Clustering parameters

300 As noted in Sect. 2.2, several parameters need to be specified ahead of executing FCM, including the number of clusters, the distance metric to measure (dis)similarity of objects, the value of the fuzzifier, the initial fuzzy partition matrix, the maximum number of iterations, and the stopping criterion. All these parameters can affect the partition outcomes, but and

Formatiert: Block, Einzug: Erste Zeile: 2 Zeich., Abstand Vor: 0 Pt., Nach: 0 Pt.

hat formatiert: Schriftart: Kursiv

Formatiert: Block

among them the most important ones are the ~~selection of~~ cluster number, the distance metric, and the fuzziness index. A brief introduction to these parameters and methods ~~how to~~ determine their optimal values ~~will be discussed in detail~~ are given in the following sections.

2.3.1 Number of clusters (c)

305 ~~Finding-Figuring out~~ the optimal number of clusters (c) is one of the challenges in cluster analysis. The optimal number of clusters is related to the structure of the investigated dataset, and ~~it~~ has a critical impact on clustering outcomes. To our knowledge, none of the existing methods ~~has been proven to be able~~ are feasible to determine the ~~perfect-optimal~~ cluster number in all possible cases and applications.

310 The frequently used method to address this problem is to set the search range of c , ~~and~~ conducting clustering to generate solutions according to the predefined number of clusters, and then ~~choose-choosing~~ one or ~~more-several~~ clustering validity indices (CVIs) to evaluate the ~~clustering~~ outcomes. By comparing the values of CVI(s) of alternative clustering solutions obtained with different number of clusters, the appropriate c ~~is~~ could be determined accordingly.

315 In this case, a validity index is used as a fitness function to evaluate the quality of the ~~obtained~~ clustering ~~solutions-results~~ in terms of intra-cluster compactness and inter-cluster separation. In addition, CVIs play an extremely important role in automatically determining the appropriate number of clusters. Plenty of CVIs have been proposed in the past. Generally, 320 these CVIs can be divided into three categories. The first ~~category-type of CVIs~~ only ~~considers~~ the property of membership degree in the calculation, such as the partition coefficient (Bezdek and Pal, 1998) and partition entropy (Simovici and Jaroszewicz, 2002), which are also the earliest validity indices for fuzzy clustering. The main disadvantage of such CVIs is that they lack direct connection to the geometry structure of the data. ~~Therefore,~~ 325 ~~with improvements, the CVIs in the second category consider both membership degree and the geometry structure of the data in the calculation. Considering this, another type of CVIs, such as~~ Fukuyama-Sugeno index (Fukuyama, 1989), Xie-Beni index (Xie and Beni, 1991), Kwon index (Kwon, 1998) and Bouguessa-Wang-Sun index (Bouguessa et al., 2006), ~~are~~ ~~some well known examples of the second category. were proposed, which takes both~~ 330 ~~membership degree and the geometry structure of data set into consideration.~~ Given their advantages over those in the first category, we only chose CVIs belonging to the second category in this study. Different from ~~the first two types of CVIs~~ ~~those in the first two categories,~~ the third type of CVIs in the third category ~~makes~~ use of the concept of

hypervolume and density for evaluation. The fuzzy hypervolume and the average partition density (Gath and Geva, 1989) are the most popular two indices within this category. In this study, the second type of CVIs was chosen for the analysis considering its applicability to our data set.

Although ~~there're~~ there are various of CVIs, no CVI can always outperform others due to their own limitations and complexity of different datasets (Kryszczuk and Hurley, 2010; Wang et al., 2021). Generally, each CVI only attaches importance to a specific aspect or limited aspects of a clustering solution, while other aspects can be inadequately represented or even overlooked (Kryszczuk and Hurley, 2010). ~~Consequently~~ In order to overcome or at least diminish the impact from this, we adopt multiple CVIs for the evaluation in this study; ~~and a~~ among all the alternatives, the following six CVIs were chosen, ~~namely including~~ the sum of within-cluster variance (V_{SWCV} , Elbow method), Fukuyama-Sugeno index (V_{FS}), Xie-Beni index (V_{XB}), Kwon index (V_{Kwon}), Bouguessa-Wang-Sun index (V_{BWS}) and fuzzy Silhouette (FS , Campello and Hruschka, 2006). ~~This selection of CVIs is dictated by the fact that they~~ They are the most frequently used CVIs ~~referred to~~ in the literature and are reported to perform well (Bouguessa and Wang, 2004; Campello and Hruschka, 2006; Rawashdeh and Ralescu, 2012; Zhou et al., 2014). More information about these CVIs can be found in ~~the~~ Supplement S1.

With respect to the search range of ~~the number of clusters~~ c , a rule of thumb ~~for the maximum number of clusters~~ suggests that the maximum c should not exceed \sqrt{n} (n here is the number of elements in a dataset) (Ren et al., 2016; Yu and Cheng, 2002). Therefore, the search range of c ~~could be~~ set to ~~be constant in~~ $[2, \sqrt{n} + 1]$ in general. To obtain a concrete result, ~~For~~ for each c in this range, the FCM algorithm ~~will be~~ performed 50 times with the default settings ($m = 2$, metric = Euclidean distance, $\varepsilon = 1 \times 10^{-5}$). ~~and~~ The selected CVIs ~~will be~~ calculated for each repetition, and the averages of results from 50 repetitions are used for further analysis. By evaluating the variations in CVIs with different c , ~~what we believe to~~ the expected optimal number of clusters is determined.

2.3.2 Distance metric

The selection of an appropriate distance or (dis)similarity metric for clustering is also challenging, since it not only relates to the inherent structure of the investigated data ~~investigated set~~, but also depends on the analysis purpose. Various distance metrics have been proposed for measuring the (dis)similarity between each pair of objects, ~~of~~ among which the Euclidean distance is the most frequently used ~~for clustering~~ metric. As defined by Eq. 4, the

hat formatiert: Schriftart: Kursiv

hat formatiert: Schriftart: Kursiv

Euclidean distance corresponds to the true geometrical distance between two objects, ~~and~~
Most of the previous many studies ~~selected~~ adopted this metric by default ~~in for~~ FCM (Haqiqi
and Kurniawan, 2015; Nishom, 2019; Singh et al., 2013). However, Euclidean distance ~~is~~
370 ~~may~~ not always ~~the right choice~~ be appropriate. The Euclidean distance assumes that each
~~attribute~~ object is equally important during clustering, namely the data being spherically
distributed, so it is ~~very~~ sensitive to outliers (Arora et al., 2019; Dik et al., 2014). If the
~~distribution of~~ investigated data is ~~non spherical in shape~~ not spherically distributed, using
Euclidean distance ~~metric for clustering could potentially lead to unsatisfactory outcomes~~ may
375 ~~degrade the performance of clustering~~ (Arora et al., 2019; Gueorguieva et al., 2017; Vélez-
Falconí et al., 2020).

$$d(x, y) = \sqrt{\sum_{i=1}^n (x_i - y_i)^2} \quad (4)$$

~~where x and y are n -dimensional objects, with x_i and y_i denoting the i^{th} dimension of x and
 y , and \bar{x} and \bar{y} are the means of x and y in all dimensions, respectively.~~

Formatiert: Abstand Nach: 12 Pt.

380 In addition to Euclidean distance, ~~some~~ other distance metrics, such as the Manhattan
distance, the Eisen cosine distance, and the Pearson correlation distance, are used to measure
(dis)similarity (Äijälä et al., 2017; Koss et al., 2020). The Manhattan distance is also named
city block distance or taxicab distance. It computes the sum of the absolute differences
between all sets of coordinates of pairwise objects following Eq. 5, ~~and which~~ is reported to
385 ~~be~~ less sensitive to noise (Dik et al., 2014). ~~Another disadvantage of Manhattan distance is~~
~~that the results would be different if the coordinate system is rotated (Vélez-Falconí et al.,~~
~~2020). However, When if~~ the attributes are discrete or binary, the Manhattan distance is more
effective than other metrics. ~~One disadvantage of the Manhattan distance is that it depends on~~
~~the rotation of the coordinate system (Vélez Falconí et al., 2020).~~

$$d(x, y) = \sum_{i=1}^n |x_i - y_i| \quad (5)$$

~~where x and y are n -dimensional objects, with x_i and y_i denoting the i^{th} dimension of x and
 y , and \bar{x} and \bar{y} are the means of x and y in all dimensions, respectively.~~

395 The Eisen cosine and the Pearson correlation distance are both correlation-based
distance metrics. The Pearson correlation distance measures the linear dependence of two
objects, ~~and while~~ the cosine distance uses the cosine angle of two objects to measure their
(dis)similarity. ~~They Both~~ are calculated by subtracting the correlation coefficient from 1, as
defined by Eq. 6 and Eq. 7, and therefore they are invariant to the magnitudes of ~~number of~~

variables. Two objects are considered similar if they are highly correlated in terms of correlation-based distances, even though they may be far away from each other in Euclidean space. This is particularly beneficial when dealing with mass spectrometric data (mass profiles). Thus, the cosine distance is commonly used to measure the (dis)similarity of aerosol source profiles (Äijälä et al., 2017; Bozzetti et al., 2017; Heikkinen et al., 2021; Ulbrich et al., 2009). It should be noted that even though correlation-based metrics are called as “distance”, strictly speaking, they are (dis)similarity metrics rather than distance metrics because they do not satisfy the triangle inequality anymore (Kaufman and Rousseeuw, 2009).

$$d(x, y) = \sqrt{\sum_{i=1}^n (x_i - y_i)^2} \quad (4)$$

$$d(x, y) = \sum_{i=1}^n |x_i - y_i| \quad (5)$$

$$d(x, y) = 1 - \frac{|\sum_{i=1}^n x_i y_i|}{\sqrt{\sum_{i=1}^n x_i^2} \sqrt{\sum_{i=1}^n y_i^2}} \quad (6)$$

$$d(x, y) = 1 - \frac{\sum_{i=1}^n (x_i - \bar{x})(y_i - \bar{y})}{\sqrt{(\sum_{i=1}^n (x_i - \bar{x})^2)} \sqrt{(\sum_{i=1}^n (y_i - \bar{y})^2)}} \quad (7)$$

where x and y are n -dimensional objects, with x_i and y_i denote the i^{th} dimension of x and y , and \bar{x} and \bar{y} are the means of x and y in all dimensions, respectively.

Since it is difficult to know the inherent structure of high-dimensional data we make use of CVIs to find the suitable distance metric of FCM for our dataset. By running FCM with all four different distance metrics mentioned above and calculated the six CVIs accordingly while retaining all other parameters, we get four parallel results for each CVI, and the optimal distance metric is determined by comparing the outcomes.

As mentioned above, since the Euclidean distance can be severely affected by the scale of objects, which means that the (dis)similarity between objects measured by Euclidean distance might get skewed if input variables are in different scales or units. Therefore, it is highly recommended to normalize the data before clustering, if Euclidean distance is chosen as a metric of (dis)similarity. In this study, we also intend to want to scale the data to directly compare the time behaviors of different variables directly, regardless of their differences in absolute intensity or detection sensitivity. In this study, therefore, we normalize the time-series data by using the Euclidean norm before clustering to eliminate the effects of different branching ratios and sensitivity of species, and to facilitate the comparison of different make their time patterns easily comparable.

430 Since it is difficult to know the inherent structure of high-dimensional data, we also make use of CVIs to figure out the suitable distance metric for FCM applied to our dataset. By running FCM with four different distance metrics mentioned above and then calculating the six CVIs accordingly while retaining all other parameters, we get four parallel results for each CVI. The “optimal” distance metric is determined by comparing these outcomes. Again, for each distance metric under scrutiny, the FCM algorithm was repeated 50 times to ensure reliable outcomes. The averages of results from these runs are then utilized for subsequent analysis.

435 2.3.3 Value of fuzzifier

The fuzzifier ($m, m \in [1, \infty)$) defines the fuzziness degree of the clustering. A proper value of m can suppress the noise and smooth the membership function (Huang et al., 2012). When $m = 1$, FCM is equivalent to the k -means algorithm. The closer m is to 1, the crisper the resulting solution becomes. On the contrary, as m becomes larger, the clustering outcomes become fuzzier. When m approaches infinity, different cluster centers and the centroid of all objects will coincide, and thereby all objects have the identical membership degree to each cluster, namely $u_{ij} = 1/c$. Theoretically, the larger m is, the fuzzier the clustering outcomes would be (Hammah and Curran, 1998). Therefore, m should be selected to fulfill the request of maximum recognition of a partition with a fuzziness as small as possible.

445 According to previous studies, the optimal value of m varies in the range of 1 to 5 (Hathaway and Bezdek, 2001; Huang et al., 2012; Ozkan and Turksen, 2007; Pal and Bezdek, 1995; Wu, 2012), and it is often set to be 2, as default value as recommended by Pal and Bezdek (1995). However, it is reported that in many cases the true value of m deviates from this recommended value, which is believed to be biased by the data structure of interest (Huang et al., 2012; Hwang and Rhee, 2007; Schwämmle and Jensen, 2010; Yu et al., 2004; Zhou et al., 2014). A few methods have been proposed to determine the optimal value or range of the fuzzifier (Gao et al., 2000; Huang et al., 2012; Ozkan and Turksen, 2007; Schwämmle and Jensen, 2010). However, they are either empirical or only applicable for limited cases, and it is still an open problem to determine the appropriate fuzzifier value in FCM.

455 In this study, we adopted the method proposed by Gao et al. (2000) to determine the optimal fuzzifier value m^* , which is based on the fuzzy decision-making theory. By constructing the Based on their method, a fuzzy objective function (μ_G) and the a fuzzy constraint function (μ_C) have been defined, the determination of m^* is transformed into a

460 ~~constrained non-linear optimization problem~~, and the intersection of μ_G and μ_C is supposed to be ~~the value of m^* the optimal solution according to the decision making theory, as defined by (Eq. 108)~~;

$$m^* = \arg \left\{ \max_{\forall m} \{ \min \{ \mu_G(m), \mu_C(m) \} \} \right\} \quad (8)$$

Where μ_G is a fuzzy objective function, as calculated by Eq. 9:

465 Since a better partition comes with a smaller sum of within cluster variation and a larger between cluster separation, the fuzzy objective G is defined as minimizing the objective function $J_m(U, V)$ as given by Eq. 8, while the fuzzy constraint C is defined as minimizing the fuzzy partition entropy $H_m(U, c)$ as given by Eq. 9. The intersection of G and C is taken as m^* , as shown in Fig. 3a, which satisfies minimizing $J_m(U, V)$ and $H_m(U, c)$ simultaneously with maximum membership degree (Gao et al., 2000).

$$\mu_G(m) = \exp \left\{ -\alpha \times \frac{J_m(U, V)}{\max_m(J_m(U, V))} \right\} \quad (89)$$

where α is a constant larger than 1, and generally set to be 1.5 in practice, and $J_m(U, V)$ is the objective function of fuzzy clustering as shown in Eq. 1.

And μ_C is a fuzzy constraint function as defined by

$$475 \mu_C(m) = \left\{ 1 + \beta \times \left(\frac{H_m(U, c)}{\max_m(H_m(U, c))} \right) \right\}^{-1} \quad (910)$$

where β is a constant that is usually set to be 10 in practice, and $H_m(U, c)$ is the fuzzy partition entropy calculated by

$$m^* = \arg \left\{ \max_{\forall m} \{ \min \{ \mu_G(m), \mu_C(m) \} \} \right\} \quad (10)$$

$$H_m(U, c) = -\frac{1}{n} \sum_{i=1}^c \sum_{j=1}^n u_{ij} \cdot \log_a(u_{ij}) \quad (11)$$

480 where u_{ij} is the membership degree of object j to the i^{th} cluster, and a is a constant $\in (1, \infty)$ which is usually set to the mathematical constant.

Based on the fuzzy decision-making method, we search for m^* in the range of [1.1, 9] with an increment of 0.1. The number of clusters varies between 2 and 10, and the initial fuzzy partition matrix (U^0) is randomly created. Other parameters are fixed. For each setting, the algorithm will is run 100-50 times for dependable results. By evaluating the variations of m^* with c and the initial values of membership degree, the optimal value of m is determined.

Formatiert: Einzug: Erste Zeile: 0 Zeich.

hat formatiert: Schriftart: Kursiv

Formatiert: Links

2.3.4 Other parameters and constraints

We find that when using a small number of iterations, FCM does not always return the same result for each run, and sometimes not even a valid solution. ~~In the first case, it seems that the algorithm converges on one local minimum with several local minima existing, while in the second case~~ This is probably because the limit of iterations is reached before the algorithm converges. To avoid ~~these two situations~~ this, the maximum number of iterations was set to be 10000 in this study. In our case, however, hundreds of iterations can already ensure a valid solution and reproducible results ~~for our data~~.

~~The initial fuzzy partition matrix was randomly created by the algorithm and 50 repetitions were used to evaluate the influence of U^0 on clustering outcomes. As for the stop criterion, the algorithm can offer reproducible results when this value is set to 1×10^{-3} or smaller. For the calculation of results selected for analysis in this study, the stop criterion was set to 1×10^{-5} .~~

The clustering results of FCM ~~are~~ not as clear as that of *k*-means clustering, in which each object is forced to one cluster exclusively. Consequently, it is important to distinguish an invalid cluster and thereby to identify an invalid solution. According to the definition of the fuzzy clustering algorithm ($\sum_{i=1}^c u_{ij} = 1$), each object can only belong to one cluster with a membership degree larger than 0.5. Therefore, we define a cluster with at least one object having the membership degree larger than 0.5 as a valid cluster, and a solution without any invalid clusters as a valid solution. In this work, only valid solutions were considered for further analysis.

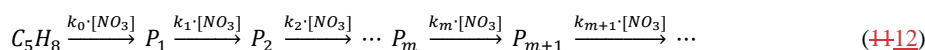
~~The initial fuzzy partition matrix was randomly created by the algorithm and 50 repetitions were used to evaluate the influence of U^0 on clustering outcomes. As for the stop criterion, the algorithm can offer reproducible results when this value is set to 1×10^{-3} or smaller. For the calculation of results selected for analysis in this study, the stop criterion was set to 1×10^{-5} .~~

2.4 Gamma kinetics parameterization (GKP)

The mass spectrometric data from chamber oxidation experiments not only contain chemical composition information of the products but also a great deal of kinetic clues. The kinetic information, mainly the reaction rate constant and the generation number (the oxidation steps needed to produce the target compound) underlying in the time series of each species, are ~~helpful~~ useful for mechanism development. However, it is challenging to extract kinetic

information from time-series data, and there is only a limited number of studies which
 520 ~~involve include~~ determination of kinetic parameters based on gas-phase measurements (Koss
 et al., 2020; Zaytsev et al., 2019). In this study, we try to determine the kinetic parameters
 based on time-series data using the gamma kinetics parameterization (GKP~~,-~~), ~~which The~~
 525 GKP model describes the multistep reaction system as a linear system with first-order
 reactions, and it was originally used in biological and chemical fields (Zhou and Zhuang,
 2007). The model returns the so-called effective rate constant (overall rate of reactions in the
 pathway) and the generation number that are implied by the time behaviors of individual
 species (Koss et al., 2020; Zhou and Zhuang, 2007). The GKP model was introduced for
 atmospheric chemistry studies by Koss et al. (2020) and has been successfully applied to
 parameterize the kinetics of gas-phase products formed from toluene and 1,2,4-
 530 trimethylbenzene oxidation in chamber studies (Koss et al., 2020; Zaytsev et al., 2019).

According to the GKP method, the NO₃-initiated isoprene oxidation system can be
 described by Eq. ~~11~~12:



where k_m is the rate constant of product P_m reacting with the NO₃ radical, and the subscript
 535 m ~~denoting denotes~~ the number of oxidation steps (by NO₃) needed to form product P_m .

Typically, the rate constants for different reaction steps are disparate, and ~~there is no~~
~~simple analytical solution for~~ the differential equations that describe Eq. ~~11~~12 ~~are~~
~~mathematically unsolvable~~. ~~However, By if~~ assuming a single rate coefficient for all steps in
 a sequence, the differential equations in Eq. ~~11~~12 become mathematically solvable.
 540 Additionally, the bimolecular reactions between P_m and NO₃ must be reduced to pseudo-first-
 order reactions by replacing the reaction time t with the integrated NO₃ exposure $\int_0^t [NO_3] dt$.

The time series of P_m can then be described by Eq. ~~12~~13 (Koss et al., 2020):

$$[X_m](t) = a(k[NO_3]\Delta t)^{m_G} e^{-k[NO_3]\Delta t} \quad (13)$$

where a is a scaling factor that relates to the product yield as well as to the instrument
 545 sensitivity (Koss et al., 2020), k is a second-order rate constant (cm³ molecule⁻¹ s⁻¹), and
 m_G is the generation number.

3. Results and discussion

3.1 Evaluation of clustering parameters

As ~~already noted above~~mentioned earlier, one of ~~the biggest challenges of the major hurdle in~~ using FCM is ~~that the necessity to predefined~~ several parameters ~~need to be predefined, and~~ ~~that~~ inadequate selection of ~~these~~ parameters can result in unreasonable clustering outcomes. The number of clusters, the distance metric and the fuzziness value are the most important ~~ones among all the~~ parameters that affect the partition. Therefore, in this section we will have a close look at these three parameters and evaluate their effects on the quality of clustering based on the methods introduced in Sect. 2.3, ~~and finally determine the~~The optimal values of these parameters ~~are then determined~~ for the analysis of our data.

3.1.1 Number of clusters (c)

To explore the effect of cluster number on partition results, we ~~ran~~applied the FCM algorithm ~~to the chamber data with c varying from 2 to 10. For each c in this range, the~~ algorithm was run 50 times and the selected CVIs were calculated accordingly for each repetition~~50 times for each c in the search range and calculated the corresponding CVIs.~~ Despite ~~small some~~ variations in ~~some specific~~ CVIs among different repetitions, the ~~tendency trends~~ of CVIs with changing cluster number and the optimal number of clusters indicated by each CVI are ~~always generally~~ the same for each repetition. ~~Therefore, we only choose the results from one of the 50 repetitions for further evaluation.~~

Figure 1 depicts different CVIs as a function of number of clusters based on FCM results from ~~one of the~~50 repetitions. For the sum of within-cluster variance (V_{SWCV}), the ~~point of inflection~~ ~~point in of~~ the curve (so-called “elbow” point) indicates the best value of c , which is in our case 5 (Fig. 1a). The Fukuyama-Sugeno index (V_{FS}) uses the discrepancy between compactness and separation of clusters to measure the quality of a clustering solution (as defined by Eq. S2), ~~and thus a~~ smaller value of V_{FS} indicates a better partition (Fukuyama, 1989). In our case, the ~~78~~ 8-cluster solution is the best option ~~suggested by in terms~~ of V_{FS} (Fig. 1b), ~~while the 5-cluster solution seems to be a local optimum.~~ Xie-Beni index (V_{XB}) is defined as the ratio of compactness and separation ~~by~~ (Eq. S3S6), where the within-cluster compactness is measured by the sum of the within-cluster variance, while the between-cluster separation is measured by the minimum squared distance between cluster centers. Generally, the smaller V_{XB} ~~is~~, the better a clustering solution can be, since under such conditions, objects within one cluster are much closer to each other but farther away to those

hat formatiert: Schriftart: Kursiv

580 in other clusters (Xie and Beni, 1991). According to Fig. 1c, $c = 2$ is the best option in terms
of V_{XB} . However, when $c = 2$, the V_{SWCV} value is relatively large (Fig. 1a), which is not
expected for a good clustering solution. When $c = 5$, the V_{XB} reaches a local minimum, and
the V_{SWCV} curve also gets the maximum curvature at this point, indicating that the local
optimal cluster number ~~is also~~ might be 5 indeed. The Kwon index (V_{kwon}) is a modification
of V_{XB} , which introduces a ~~punishing-penalty~~ function additionally to measure the cluster
585 compactness together with the sum of within-cluster variance. As defined by Eq. ~~S4S8~~, the
~~punishing-penalty~~ function measures the average squared distance between cluster centers
and the overall mean of the dataset. By introducing this factor, V_{kwon} eliminates the
monotonous decreasing tendency when c approaches the number of objects in the dataset
(Kwon et al., 2021). Like V_{XB} , a smaller V_{kwon} indicates a better partition, and the results in
590 Fig. 2d show that the local optimal value of c is ~~as well 5 as well~~.

hat formatiert: Schriftart: Kursiv

hat formatiert: Schriftart: Kursiv

Figure 1. Values of selected clustering validity indices V_{SWCV} (a), V_{FS} (b), V_{XB} (c), V_{Kwon} (d), V_{BWS} (e), and FS (f) as a function of the number of clusters from 2 to 10. The averages of results from 50 repetitions are shown in the plot, and the error bars show the standard deviations. Blue points denote the optimal values of c according to each CVI, and larger red hollow circles indicate the solution selected for further analysis is marked by red circles.

In addition, ~~we calculated~~ the Bouguessa-Wang-Sun index (V_{BWS}) and the Fuzzy Silhouette values (FS) were calculated for each FCM run. These two indices use slightly different definitions of compactness and separation to measure the quality of clustering. The V_{BWS} uses the fuzzy covariance matrix as a measure of compactness, and thus V_{BWS} takes cluster shape, density, and orientation into account and has been proven to work well for largely overlapping clusters (Bouguessa et al., 2006; Bouguessa and Wang, 2004). In general, the larger V_{BWS} is, the better a fuzzy partition will be, and hence the optimal number of clusters for our data is 3 (and 4) based on V_{BWS} (Fig. 1e). Meanwhile, as depicted in Fig. 1e, V_{BWS} shows that there is a local optimum with at $c = 7$, though it has a higher uncertainty at this this point. ~~As for FS , it~~ is an extension of the concept of Crisp Silhouette (CS) that was originally developed to assess non-fuzzy clustering (Rousseeuw, 1987). ~~FS -It~~ is more appealing than CS for fuzzy clustering since it makes explicit use of the fuzzy partition matrix. In FS , objects in the near vicinity of cluster centers are given more importance than those located in the boundary region (overlap). Consequently, it performs better than CS for highly overlapping data (Campello and Hruschka, 2006). In principle, a larger overall FS suggests a better partition. Therefore, the best number of clusters determined by FS is 2 (Fig. 1f). Nevertheless, when $c = 2$, the sum of the within-cluster variance for this solution is still quite high (Fig. 1a), which is not expected for a good partition. ~~However, it looks reasonable~~ It seems more sensible to set the number of clusters to 5, as this is where FS reaches its local maximum and V_{SWCV} is significantly reduced and has the maximum curvature, which corresponds to the local maximum in terms of FS . It is worth noting that the silhouette score can not only be used to assess the overall quality of partition, but also to evaluate the quality of individual clusters and objects. The silhouette score of an object ranges from -1 to +1, and a value close to +1 indicates that the object is correctly assigned. On the contrary, a silhouette value of -1 implies that the object is misclustered and should be assigned to a neighboring cluster. A silhouette value approaching 0 suggests that the object is in the overlapping region of clusters, and thus the algorithm is unable to assign it to one cluster (Campello and Hruschka, 2006; Rawashdeh and Ralescu, 2012; Subbalakshmi et al., 2015).

hat formatiert: Schriftart: Kursiv

hat formatiert: Schriftart: Kursiv

In summary, different CVIs sometimes suggest a different optimal cluster number. However, by making use of information from multiple CVIs, the appropriate number of clusters in this study is determined to be 5. It should be noted that the main topic of this study is to offer a proof of concept for the application of FCM in deconvolution of mass spectrometric data. Therefore, the depth of the discussion about the determination of the correct cluster number in this section must suffice for our purpose, ~~and the~~ The value solution of $c=5$ is selected here as one example for the chemical characterization and kinetic parameterization in the following sections. In addition, It should also be noted is worth mentioning that the multiple CVIs method presented in this section provides a way to automatically determine the optimal number of clusters for FCM.

3.1.2 Distance metric

Figure 2 shows four selected CVIs as a function of c with different distance metrics. As ~~a quick reminder mentioned before~~, smaller V_{FS} and V_{Kwon} indicate better partitioning, whereas for V_{BWS} and FS , the opposite applies. In terms of V_{FS} , it indicates that the cosine distance is more suitable for FCM in our case, although the effects of using impacts of different distance metrics on the clustering outcomes are ~~negligible minimal~~ (Fig. 2a). ~~However, different results arise when using V_{BWS} (Fig. 2e).~~ The V_{BWS} values also suggest that the cosine distance ~~seems is~~ more appropriate for FCM regarding the data used in this study. ~~Currently the reason for this is not clear.~~ As for V_{Kwon} and FS , there are no significant differences in the quality of partitioning when the number of clusters is small (e.g., $c = 2, 3, 4$) despite different distance metrics, as shown in Fig. 2b and Fig. 2d, ~~but~~ However, the discrepancies become more pronounced with increasing c . In general, the Euclidean distance is more appealing for our data, ~~especially for c with a value of 5, which is the appropriate cluster number determined in Sect. 2.3.4 in terms of V_{Kwon} and FS .~~ Consequently To conclude, we conclude that among all the examined distance metrics ~~tested~~, the Euclidean and cosine distance provided a better performance in seems the most appropriate choice for fuzzy clustering regarding the data used in this study, and the Euclidean distance was employed as the (dis)similarity metric in FCM for further analysis in this study. Additionally, the Euclidean distance was used in the calculation of various CVIs.

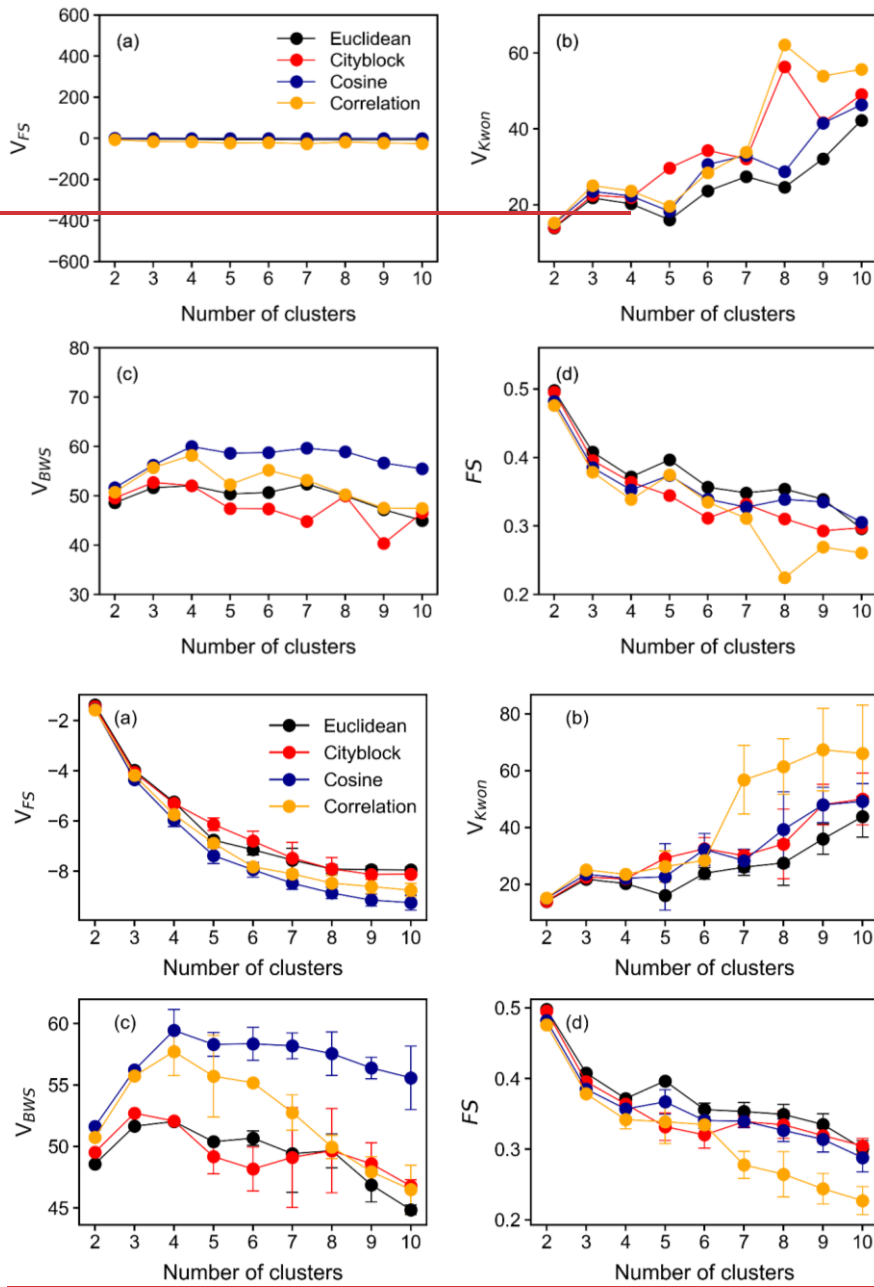


Figure 2. Values of selected clustering validity indices V_{FS} (a), V_{Kwon} (b), V_{BWS} (c), and FS (d) as a function of the number of clusters. Points in different colors indicate results

660 obtained with different distance or similarity metrics. The averages of results from 50 repetitions are shown in the plot, and the error bars denote the standard deviations. Euclidean distance was used in the calculation of CVIs.

3.1.3 Fuzzifier value

665 Based on the fuzzy decision-making method introduced in Sect. 2.3.3, we searched m^* in the range of [1.1, 9] with an increment of 0.1. The intersection of the fuzzy objective function, $\mu_c \mathcal{G}$, and the fuzzy constraint, $\mu_c \mathcal{C}$, as shown in Fig. 3a, indicates the optimal value of the fuzzifier for each run. To investigate whether m^* ~~is dependent~~ depends on c and/ U^0 ~~or on the initial values of the membership degree~~, the number of clusters was set to vary from 2 to 10. For each c in this range, FCM was performed ~~100-50~~ times with a randomly created initial fuzzy partition matrix (U^0) .

670 As shown in Fig. 3b, we do observe a relationship between m^* and c/U^0 . For smaller cluster numbers, ~~(e.g., $c = 2$ or 3),~~ the determined optimal values of m are slightly larger than those obtained ~~for~~ with larger c ($c \geq 4$). In addition, the results obtained with a smaller ~~c number of clusters~~ are more robust. Different repetitions always return identical m^* , which suggests that the initial fuzzy partition matrix does not affect m^* when the number of clusters is smaller than 4. However, when c increases to 4 or even larger ~~values~~, there is a variation in m^* among different repetitions, indicating that U^0 starts to affect the determined value of m^* , even though the variation of the value of m^* is small (between 1.42 and 1.52). ~~It is not clear why different numbers of clusters have such distinct effects on m^* , and answers for this question are outside the scope of this work.~~ One plausible explanation for the dependency of m^* on c/U^0 is shown as follows. When c is small, there are more overlaps between clusters and thus m^* can be relatively large. When c becomes larger, the assignment becomes “stricter” and the overlaps between clusters are reduced. Therefore, m^* gets smaller, and the clustering outcomes become more specific, which are likely to be more sensitive to local minima. Since the local minima largely depends on U^0 , consequently, the results become more sensitive to U^0 .

675
680
685

hat formatiert: Schriftart: Kursiv

hat formatiert: Schriftart: Kursiv

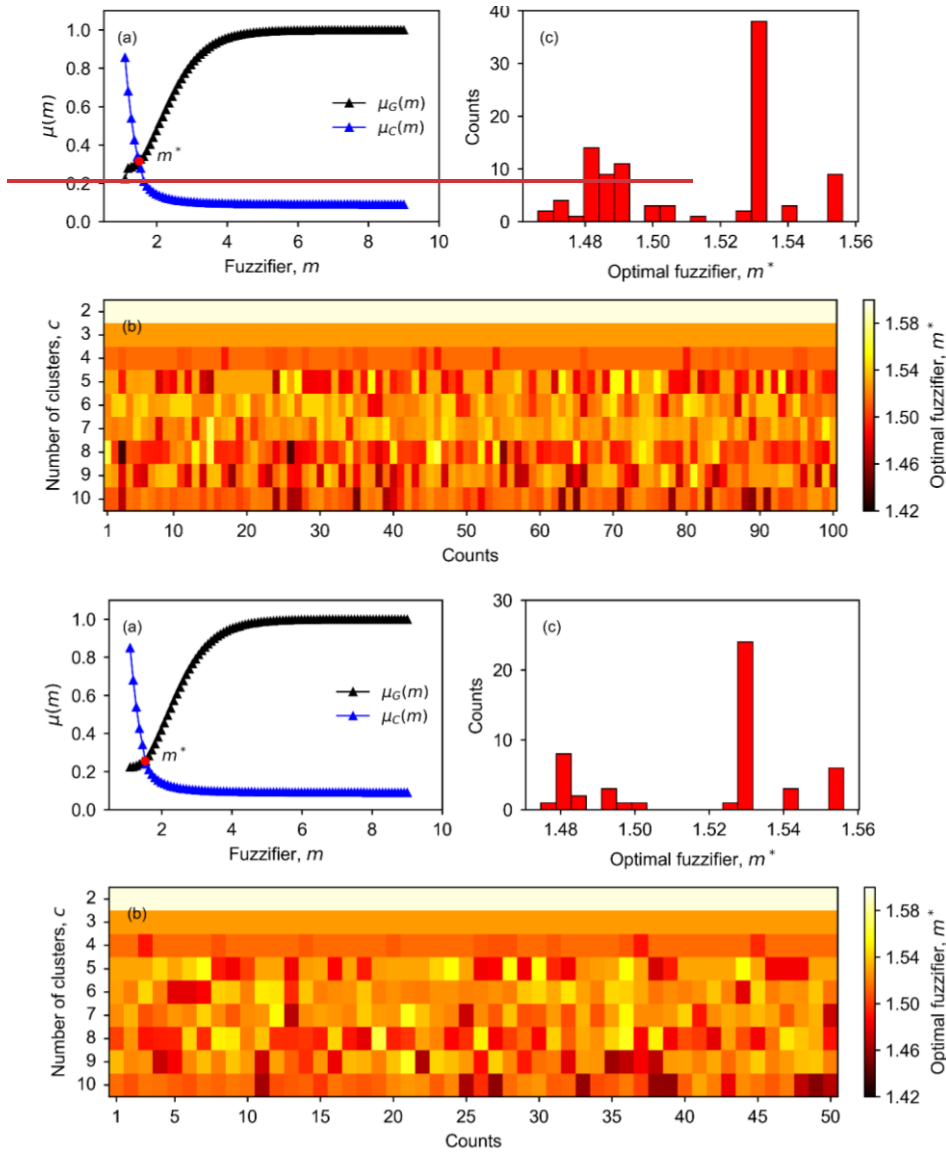


Figure 3. Determining the optimal value of the fuzzifier (m^*) in FCM. In panel (a), the intersection (red point) of the fuzzy objective function (μ_G) and constraint (μ_C) is determined as m^* . Panel (b) depicts the relationship between m^* , the number of clusters (c), and the initial fuzzy partition matrix (v^0). Panel (c) shows the frequency distribution of m^* for ~~100~~ 50 repetitions with $c = 5$ (determined as the optimal number of clusters in this study).

690

Figure 3c displays the distribution of m^* obtained from ~~100-50~~ repetitions with $c = 5$. The histograms of the optimal value of m with other numbers of clusters are provided in the supplement (Fig. S3). For $c = 5$, the results suggest that the optimal value ~~for~~ of m is 1.53 in most cases. Therefore, a value of $m = 1.53$ is used for the FCM in this study.

Overall, the number of clusters and the initial membership degree matrix do affect the optimal value of the fuzzifier that was determined based on the fuzzy decision-making method in this study, but the influence is not very strong. The values of m^* determined for our data set vary around 1.5 despite different c and U^0 , indicating that the FCM results in this study are relatively crisp.

hat formatiert: Schriftart: Kursiv

3.2 FCM clustering results

3.2.1 FCM of chamber data

Using the appropriate clustering parameters determined in Sect. 2.3, we performed FCM ~~on~~ to chamber data with the number of clusters varying from 2 to 10. For each ~~case~~, the algorithm was run 50 times. According to the results of these 50 repetitions, two- and three-cluster solutions seem very robust. The repetitions always gives identical outcomes despite different initial partition matrices. This is also true for the five-cluster case. However, the influence of the initial position of the cluster centers on the partition increases when the number of clusters is further increased, but in all cases, at least more than half of the repetitions return the same results; thus, we select the most frequent outcomes as the final clustering results solutions for each case. Here we will not describe all solutions in detail, but instead, try to formulate a synthesis of the results and present the common features shared by solutions with different numbers of clusters.

hat formatiert: Schriftart: Kursiv

Figure 4 shows the FCM results with 2-5 clusters ~~of~~ for the chamber data obtained during the isoprene-NO₃ experiment. Additional solutions with 6-10 clusters are shown in the Supplement (Fig. S4). Two distinct clusters emerge from the data ~~for~~ in the two-cluster solution. According to their relative formation rates, cluster 1 is regarded as first-generation cluster since species belonging to this cluster show a pronounced signal increase after addition of the reactants, while cluster 2 behaves more like second or later-generation products with its overall formation rate being much smaller ~~compared to~~ than that of cluster 1. In addition to the time patterns, the mass profiles of cluster 1 and cluster 2 are clearly different (Fig. 4b).

725 When the cluster number is increased to 3, both, the time pattern and the mass profile of
cluster 1, almost remain unchanged compared to those in the two-cluster case. It seems that
mainly the former cluster 2 is separated into two new clusters (cluster 2 and 3) with different
formation rates for each. Accordingly, ~~cluster 2~~ is regarded as a representative of the
second-generation processes, and cluster 3 represents third- or later-generation products since
it exhibits a smaller formation rate compared to cluster 2. However, ~~the narrowing of the~~
730 ~~there are less high-affiliation~~ ~~cluster~~ members (with a membership degree over 0.5) ~~of in~~
cluster 1 ~~in the three-cluster solution, suggests indicating~~ that at least some of the former
contributors of this cluster have been moved, most likely to the new cluster 2. The mass
profiles of cluster 2 and cluster 3 display quite distinct features, as shown in Fig. 4b, but the
mass profiles of ~~the two-cluster 2 of in both~~ the two- and the three-cluster solution match to a
735 large extent, even though their time patterns are somewhat different.

~~As shown in Fig. 4b. The effect of increasing the number of clusters from 3 to 4 can be~~
~~best seen in the mass profiles (Fig. 4b). Part of the species from the former cluster 1 in the~~
~~three-cluster solution is separated out as to a new cluster 2 (cluster 2 in four-cluster solution)~~
~~when increasing the number of clusters from 3 to 4. The newly formed cluster shares the~~
740 ~~same fingerprint molecules, i.e., C₅H₉NO₅ and C₅H₉NO₆ (corresponding to species no. 34~~
~~and no. 38 in Fig 4b), in the mass profile with cluster 1 in three-cluster case dominated by~~
~~molecule(s) from a very narrow mass range, where mass profile 1 also has its maximum.~~
This migrates the former cluster 2 into cluster 3, and cluster 3 into cluster 4, ~~with some slight~~
~~alterations in their time patterns and mass profiles shown also by the according mass profiles~~
745 ~~3 and 4.~~ The time series of the new cluster 2 resembles that of cluster 1, but with ~~slowed~~
~~down~~ ~~smaller~~ formation rates. In general, ~~for all clusters~~ the member traces ~~of different~~
~~clusters~~ seem to converge towards the time traces of the cluster centers, indicating that the
system approaches the correct number of clusters.

When increasing the number of clusters from 4 to 5, ~~the a new, distinct~~ cluster (cluster 5)
750 ~~that~~ emerges, ~~which~~ has very small production in the early reaction stage, and its time trace
shows that members in this cluster ~~are were~~ destroyed ~~very fast~~ ~~significantly~~ when there ~~is~~
~~was~~ abundant NO₃ in the system (Step IV in Fig. S1). This specific character in time seems to
evolve already in cluster 4 ~~of in~~ the four-cluster solution. ~~As shown in Fig. 4b, the~~ The mass
profiles of the first four clusters of the five-cluster solution are very similar to those of the
755 four-cluster case, but the mass profile of cluster 5 shows distinct differences from that of the
others. It ~~is important to mention should be noted~~ that these ~~5 five~~ clusters ~~represent~~ now also
~~effectively capture~~ the loss rates ~~at over~~ a time scale larger than 13h ~~reasonably well~~, and that

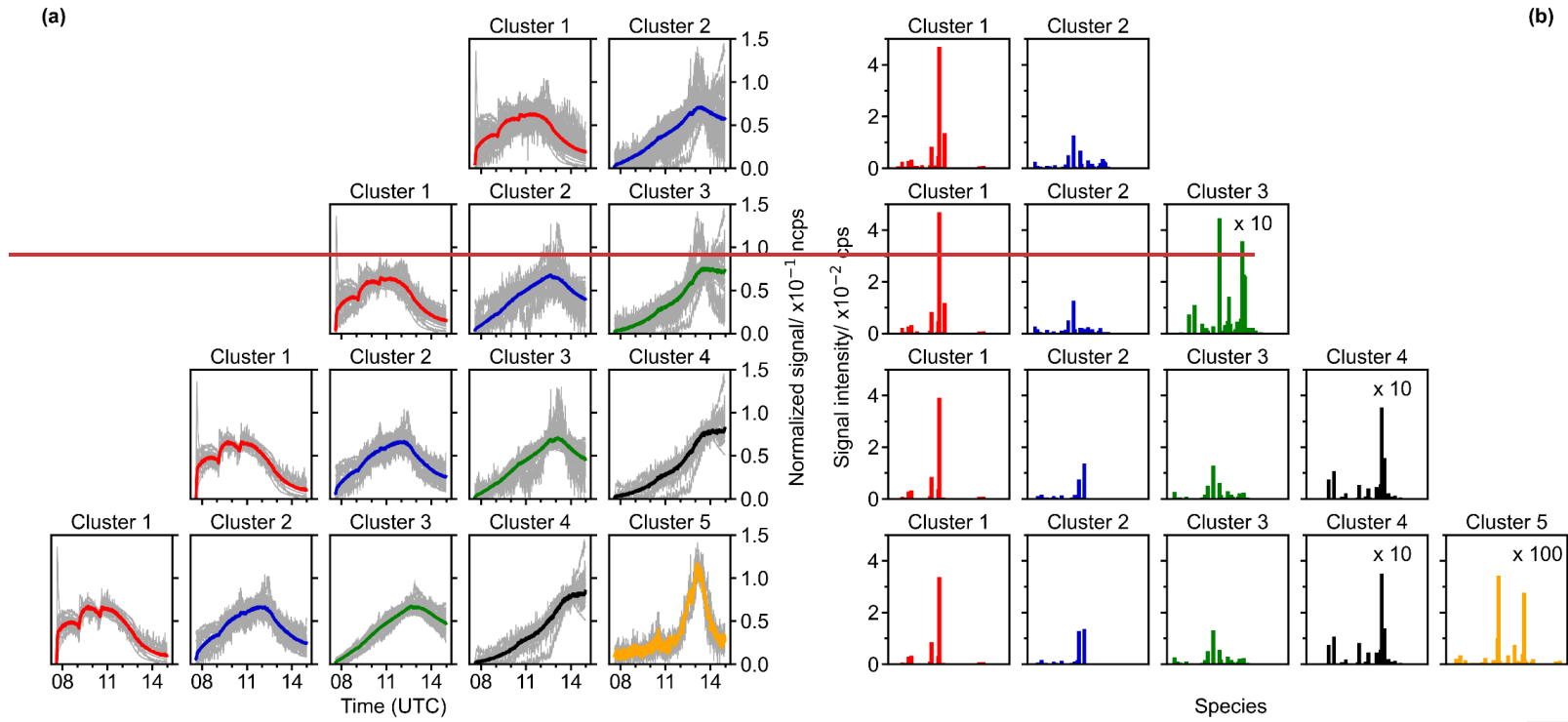
~~most the~~ members ~~of most of the five in these~~ clusters are well represented by their respective cluster centers.

760 When the number of clusters is further increased, more detailed and complicated clustering outcomes emerge, which is impelled by different formation and/or destruction pathways of ~~individual~~ species (Fig. S4). However, the differences between the new and existing clusters become smaller. Since the major objective of this study is to demonstrate the applicability of FCM ~~for in~~ analyzing mass spectrometric data, we will not discuss the detailed interpretation of these solutions here.

765 To better understand the chemical composition of clusters, the bulk chemical properties ~~such as like~~ hydrogen-to-carbon ratio (H:C), oxygen-to-carbon ratio (O:C), and average carbon oxidation state (\overline{OS}_C) of different clusters were calculated and compared. The \overline{OS}_C of each cluster was calculated following the method proposed by Kroll et al (2011), in which all the N atoms of N-containing compounds were assumed to be present in nitrate groups (and thus $OS_N = +5$), as described in our previous study (Wu et al., 2021). Figure 5 shows the distribution of clusters in the \overline{OS}_C vs. n_c space for solutions with 2 to 5 clusters. Additional results for solutions with 6 to 10 clusters can be found in the supplement (Fig. S5). The contribution of an individual species to a cluster is weighted by its nominal mass and signal intensity in the cluster profile. Regardless of the number of clusters, different solutions cover similar chemical composition ranges in terms of average \overline{OS}_C and n_c . However, there are discrepancies in detail. For example, the \overline{OS}_C of cluster 5 in the five-cluster solution slightly deviates from the trend that the other four clusters ~~are following~~ follow. A similar behavior ~~can be is~~ observed for cluster 1 in the six-cluster solution. This indicates that increasing the number of clusters could help to find new groups of species with distinct chemical compositions. However, further increasing the number of clusters to 7 or more clusters does not ~~point out yield~~ new clusters with significantly different chemical composition, implying that $c = 5$ or 6 is the appropriate number of clusters in terms of separation by chemical composition. It is also shown in Fig. 5 that different clusters are well separated in the \overline{OS}_C vs. n_c space despite some overlaps, indicating that ~~different clusters they~~ have a distinct chemical composition. For instance, the two early-generation clusters, Even clusters with similar generation number, like cluster 1 and cluster 2 in of the four-cluster solution, are grouped into different clusters due to their different differentiated in chemical properties from each other.

780 In general, the early-generation clusters with lower oxidation degree fall in the corner of the plot with smaller \overline{OS}_C but larger n_c , while the later-generation clusters with higher

795 oxidation degree move towards the corner with larger \overline{OS}_C but smaller n_C . ~~This indicates~~ suggesting that the later-generation products detected in the gas phase in this study ~~are~~ were formed through further oxidation of early-generation species and they underwent ~~undergo~~ more fragmentation during oxidation. Of course, it is very likely that there are later-generation products with larger n_C . However, as they become highly functionalized through multiple oxidation steps, they would have a very or extremely low volatility and thus only/mostly exist in the particle phase, undetectable in the gas phase.



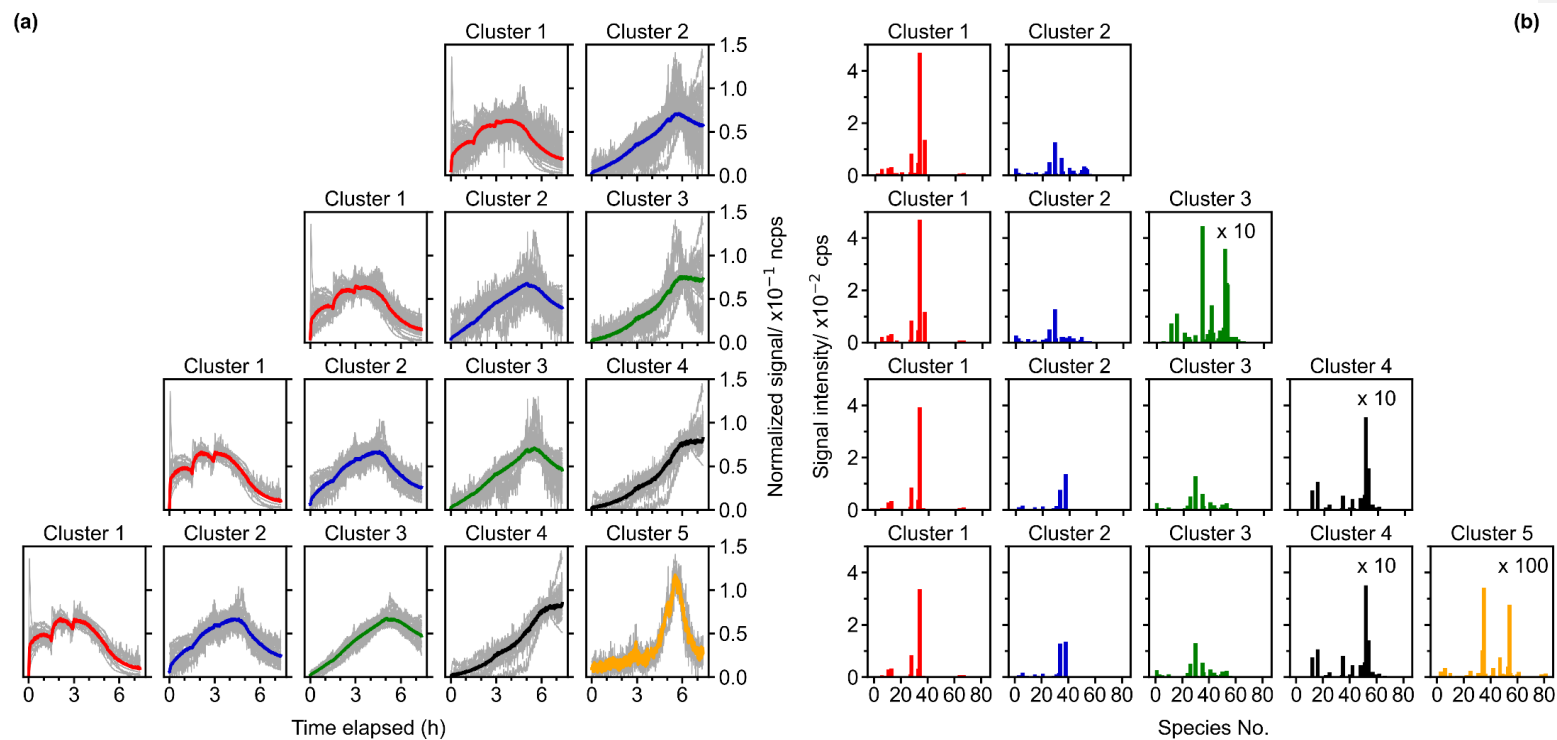
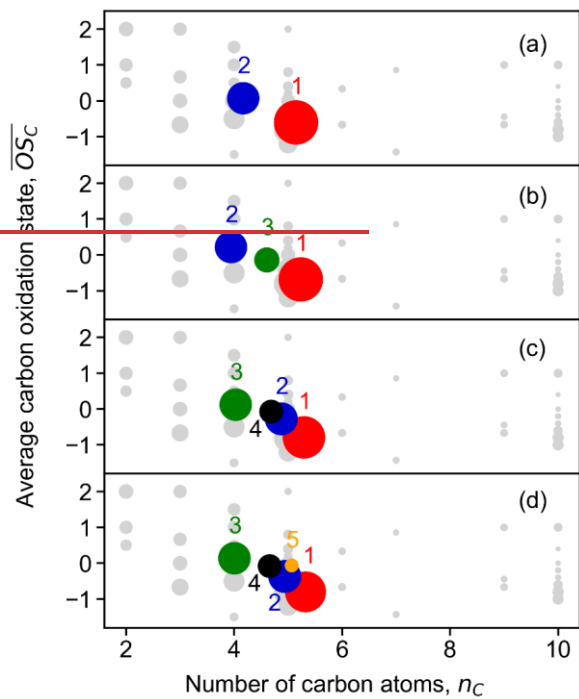


Figure 4. Results of fuzzy *c*-means clustering for chamber data with cluster numbers between 2 and 5: Time series (a) and mass profiles (b) of clusters for each solution (in row). The time series of cluster centers are shown as thick, colored solid lines, and the time series of species with the membership degree larger than 0.5 to the cluster are illustrated as thin, gray lines. [The species number in panel \(b\) corresponds to species listed in Fig. S7 \(in order of molecular mass\).](#)



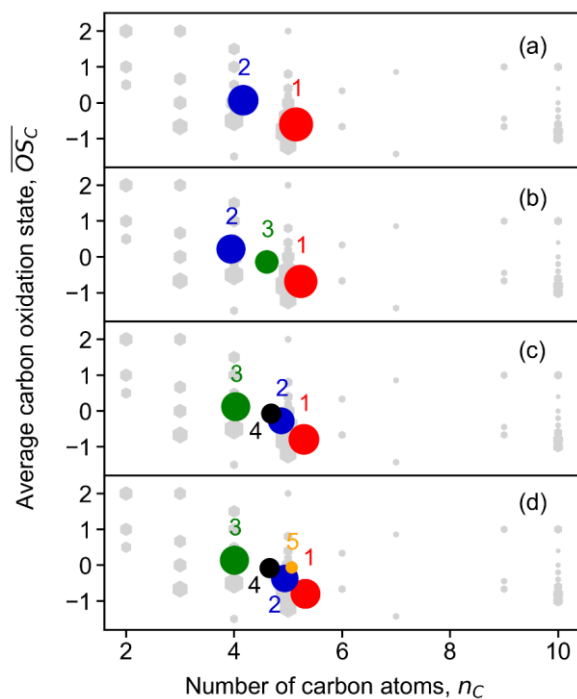


Figure 5. Average carbon oxidation state (\overline{OS}_C) of the obtained FCM clusters from chamber data as a function of number of carbon atoms (n_C). Panel (a) to panel (d) show results for solutions with 2 to 5 clusters, respectively. Cluster centers are depicted by circles in different colors. The color scheme follows that of the cluster centers in Fig. 4. The marker area of clusters is proportional to the sum of average signal intensity of all species in the cluster weighted by their membership degrees. Closed-shell products detected by Br-CIMS individual species are shown as grey circles, and the marker area is proportional to the square root of the average intensity of species the clusters over the whole experiment.

hat formatiert: Hochgestellt

3.2.2 FCM of model data

As mentioned previously, we also applied FCM onto data obtained from a box model, with the default gas-phase reaction schemes for isoprene-NO₃ taken from the MCM v3.3.1 (Jenkin et al., 2015). For consistency, only closed-shell products from isoprene oxidation in MCM are considered were taken for the clustering. Since the reaction scheme of isoprene with NO₃ in the MCM mechanism is semi-explicit, the clustering results of modelled data provides a way to evaluate the applicability of fuzzy clustering for analyzing time series analysis data. In turn, by comparing the cluster centers derived from model data with those derived from mass spectrometric data, one can check if the model can well reproduce the

825 measurements, and thus investigate the representativeness of ~~reach-oxidation~~ mechanism coupled in the model.

Figure 6 shows the results of FCM applied to model data, again with the number of clusters varying from 2 to 5. ~~From the results it becomes clear~~It is clearly shown that different species are sorted according to their patterns of time behaviors, and that different clusters represent multi-generation products. Taking the 2-cluster solution as an example, the signals of most species in cluster 1 increase evidently as soon as the reaction is initiated, while those in cluster 2 grow considerably slower, indicating that cluster 1 is a surrogate of early-generation products, whereas cluster 2 corresponds to later-generation products. This is very similar to what we observe from the real measurements, even though the time behavior derived from those two cases are not the same. ~~However, it seems that~~ the fast-forming pathways ~~are~~play a more important role in the measured data than in the model data. In addition, ~~Similarly,~~ more later-generation clusters are ~~screened~~selected out from the model data with increasing number of clusters, whilst the changes in early-generation clusters are ~~not significant~~indistinct. ~~Looking at~~However, in terms of clusters 3-5 in the five-cluster solution, it is evident that certain chemical loss processes are missing in the MCM mechanism, which are observed ~~from~~ the chamber data, ~~however. It should be noted that~~For instance, autoxidation and related processes for the isoprene + NO₃ system are underrepresented in the MCM, ~~which is also true for~~as well as the formation of accretions products.

845

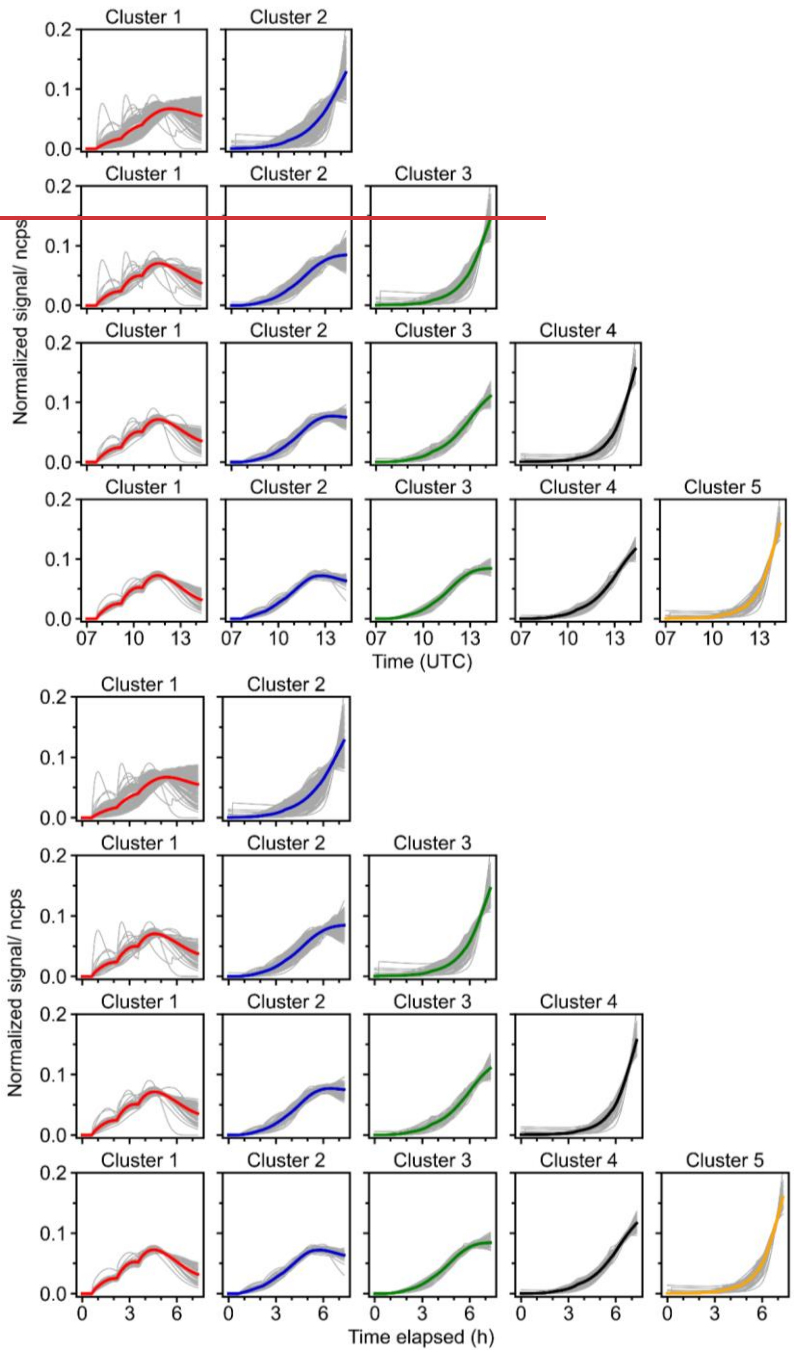


Figure 6. Results of FCM for model data with the number of clusters varying from 2 to 5. Each row represents one solution, with the time series of cluster centers shown in thick, colored solid lines, and species with the membership degree larger than 0.5 to the cluster illustrated as thin, gray solid lines.

As for the chemical properties, different clusters are discrete in the \overline{OS}_C vs. n_C space (Fig. S6), and thus ~~it can be inferred that we can conclude from the results of FCM that it will also classify~~ product species ~~would also be grouped~~ in a reasonable way when ~~applied applying FCM~~ to experimental data. Moreover, clusters in different solutions cover a similar chemical composition range of \overline{OS}_C and n_C despite increasing number of clusters (except for the two-cluster solution), well consistent with what we observed for the chamber data. However, ~~the increase in the~~ \overline{OS}_C of clusters ~~for model data decreases is~~ less pronounced during the oxidation processes ~~prominently with increasing n_C for the model data~~, probably due to the absence of ~~autooxidation steps in the MCM. Moreover, the MCM lacks~~ accretion products ~~in the MCM~~ (mostly assigned to early-generation clusters with more carbon atoms in bulk). ~~The MCM but~~ tends to ~~produce have~~ more small species (with low n_C), which is not observed in the mass spectra data. This can be due to the detection limits of the Br-CIMS for smaller compounds. Regarding the two-cluster solution, the chemical range of clusters is much narrower, and they are overlapping in the chemical space to some extent, suggesting that the number of clusters is not enough.

~~In general, a~~ According to the outcomes from the application of FCM to both measured and model data, we conclude that FCM can give interpretable and chemically meaningful results when ~~it is~~ applied to mass spectrometric data ~~for in~~ time series analysis.

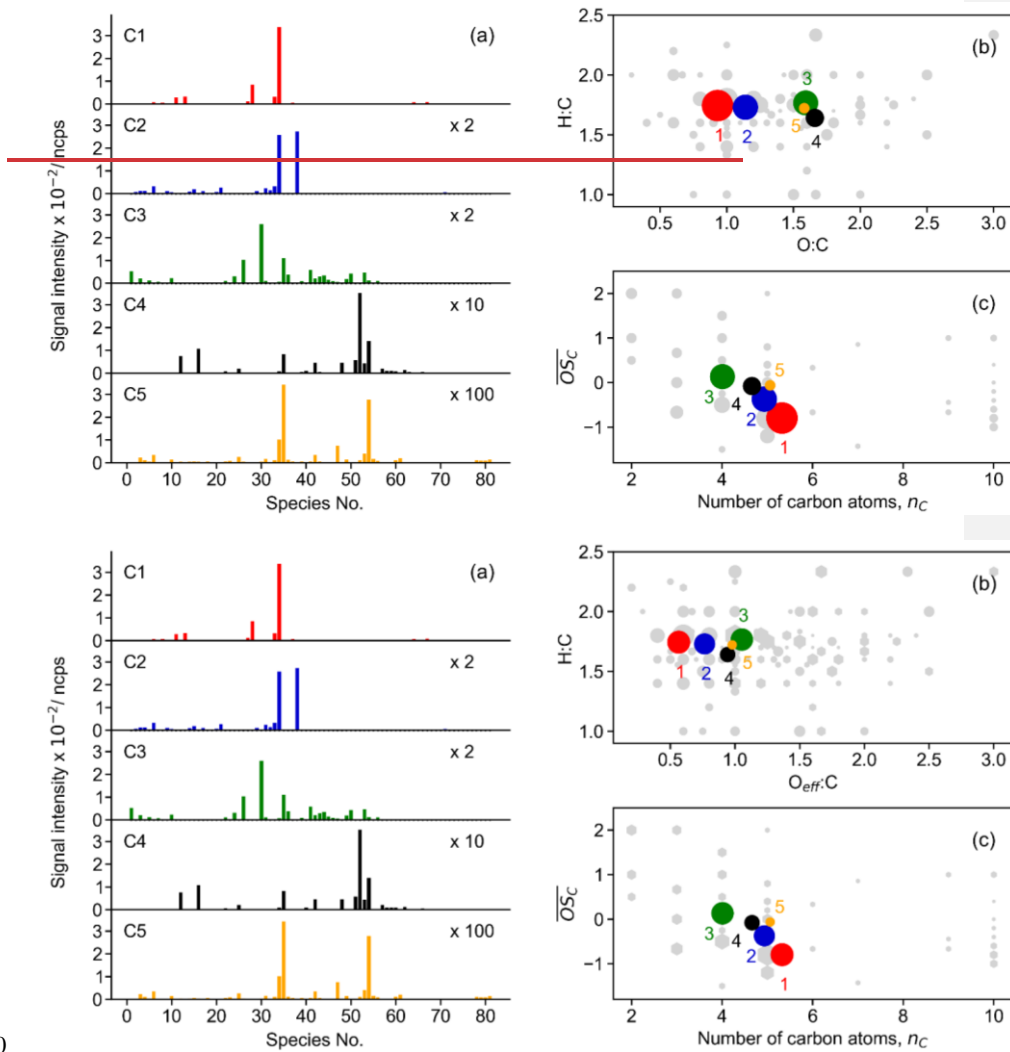
3.3 Insights from clustering results

3.3.1 Chemical properties of different clusters

In this section, ~~we will analyzeutilize~~ the five-cluster solution, ~~identified as the optimal cluster number for our dataset (Sect. 2.3), to exemplify the functionalityillustrate of how to FCM for extractextracting the~~ chemical and kinetic information ~~underlying infrom~~ the mass spectrometric data ~~based on the FCM analysis. The five-cluster solution is chosen because $e = 5$ is the mathematically optimal cluster number determined for our dataset in sect. 2.3.~~ This does not necessarily mean that ~~we claim it is the five-cluster solution is~~ superior ~~to over~~ others ~~solutions, e.g., the six-cluster solution. Besides, we confirmed~~ However, ~~as demonstrated in the previous sections, that~~ the FCM results exhibit ~~generalconsistent~~ features regardless of the ~~predefined~~ number of clusters ~~predefined, so that~~ Therefore, findings based

880 ~~on the analysis of derived from~~ the five-cluster solution ~~can hopefully also be generalized~~
~~for~~ could potentially apply to other cases.

It ~~can be~~ clearly ~~seen~~ shown in Fig. 7a that different clusters ~~have~~ are significantly different ~~in~~ compositions. For example, cluster 1, ~~which representing~~ represents the early-generation products, is dominated by a single species (with the chemical formula $C_5H_9NO_5$), and its intensity is much higher than those of the other four clusters. Another characteristic of cluster 1 is that more than 80% of detected 2N-dimers (except one species with the formula $C_{10}H_{16}N_2O_{11}$) are assigned to this cluster (Fig. S7). These compounds are obviously first-generation products ~~probably~~ formed through $RO_2 + RO_2$ reactions (Wu et al., 2021), ~~and~~ therefore, it is reasonable to sort them into cluster ~~1~~, which is representative for the early-generation products. Cluster 2 also behaves like early-generation products, but differs from cluster 1 in terms of reactivity, i.e., formation and destruction rates. The differences of cluster 1 and cluster 2 in chemical composition are even more perceptible. As shown in Fig. 7a, ~~besides $C_5H_9NO_5$, there is~~ another 1N-monomer ($C_5H_9NO_6$) ~~is~~ present in cluster ~~2~~ with a relatively high intensity ~~besides $C_5H_9NO_5$~~ . In addition, most of the detected small molecules ($C_{\leq 3}$) are assigned to this cluster (Fig. S7). Note that the formation rate of cluster 2 (~~from FCM analysis of the chamber data~~) resembles that of cluster 1 (~~in the five-cluster solution~~) ~~from FCM analysis~~ of the model data. In addition, the fractions of some 3N-dimers (e.g., $C_{10}H_{17}N_3O_{12-14}$) in cluster 2 are relatively high (Fig. S7). 3N-dimers are expected to be second or even later-generation products that are produced from the cross reaction of a first-generation nitrooxy peroxy radical and a secondary dinitrooxy peroxy radical, or from further oxidation of the corresponding 2N-dimers (Wu et al., 2021). This indicates that cluster 2 is very likely a mixture of the first- and second-generation products, which have not been resolved by FCM ~~with~~ in the five-cluster solution. Increasing the number of clusters might help to separate the typical behavior of a minority of components. When the cluster number is increased to 6, it is indeed mainly the former cluster 2 in the five-cluster solution ~~which~~ is further split into new clusters (~~cluster 2~~ and ~~cluster 3~~), in which the first-generation behavior of the new cluster 2 is more pronounced. From this point of view, the six-cluster solution seems better than the five one.



910

915

Figure 7. Chemical properties of clusters from the five-cluster solution. The subplots show mass profile of each cluster (a), van Krevelen plot (b), and average carbon oxidation state of clusters (c), respectively. Different clusters are distinguished by color, and the color scheme follows that in Fig. 4. The marker area of clusters is proportional to the sum of average signal intensity of all species in the cluster weighted by their membership degrees. The species number in panel (a) corresponds to species listed in Fig. S7 (in order of molecular mass). Grey circles-hexagons in panel (b) and panel (c) denote species identified by Br-CIMS-, and The the marker size-area is proportional to the square root of the average intensity of clusters/species over the whole experiment.

hat formatiert: Hochgestellt

920 Regarding later-generation clusters, namely cluster 3, cluster 4 and cluster 5, ~~in general~~
the second- or later-generation products, such as C4 species, 2N- and 3N-monomers, are
predominant in their composition. Nevertheless, the mass profiles of cluster 3, cluster 4, and
cluster 5 are quite distinct. For example, cluster 3 is dominated mainly by a C4 species
925 (C₄H₇NO₅), while the major fingerprint of cluster 4 is constituted by two 2N-monomers
(C₅H₈N₂O₈ and C₅H₈N₂O₉), a C4 species (C₄H₇NO₆), and a C2 species (C₂H₃NO₅). In
addition, 3N-monomers are almost completely present in cluster 4 (Fig. S7). Cluster 5 has a
much lower intensity compared to other clusters, and a distinctive characteristic of this cluster
is a high ~~attribution-contribution~~ of two 3N-dimers (C₁₀H₁₇N₃O₁₅ and C₁₀H₁₇N₃O₁₆) (Fig. S7).

930 Figure 7b and 7c show the chemical properties of ~~each cluster's center described by~~
terms of the bulk elemental molar ratios (in the Van Krevelen space), and the average carbon
oxidation state. The Van Krevelen plot visualizes the chemical composition of organics by
hydrogen-to-carbon (H:C) vs. oxygen-to-carbon (O:C) ratio, and it is widely used to trace the
origin and evolution of organic compounds (Chhabra et al., 2011). When calculating the O:C
ratios of N-containing compounds, the concept of effective oxygen number ($n_{O_{eff}}$,
935 $n_{O_{eff}} = n_O - 2 * n_N$) was employed, where in the case of a nitrate group, only one of the O
atoms bonded to C atom was considered in the calculation (Xu et al., 2021). The clusters
centers cover a narrow range of chemical space of the original dataset (grey ~~spheres-circles~~
in Fig. 7b), but are located where most of the compounds fall in. They lie almost along a line ~~for~~
of H:C = 1.75 in the Van Krevelen plot, indicating that they have gained on average one H
940 atom compared to isoprene. A trajectory with slope zero is expected in van Krevelen plots
when only alcohol or hydroperoxide functionalities are introduced in the molecule (Chhabra
et al., 2011). This is a characteristic of autoxidation steps (-O₂H) or H-shifts in alkoxy
radicals (-OH, and thereafter -O₂H). Therefore, the distribution of the clusters in the Van
Krevelen space implies that autoxidation steps or intramolecular H-shifts were involved in
945 the reactions of isoprene with NO₃ studied in this work.

In terms of average oxidation state and carbon atom numbers, the early-generation
products which undergo less oxidation steps usually have much lower oxidation degree but
more carbon atoms per molecule. With the reaction proceeding, the early-stage products will
be further oxidized and fragmented, leading to the formation of later-generation products
950 with a higher oxidation state but less carbon atoms per molecule. Consequently, the trajectory
of chemical processes generally starts with the precursor in the right lower corner and moves
towards to the left upper area (products) in the \overline{OS}_C vs. n_C space through oxidation and

fragmentation. In this study, the early-generation clusters have a lower oxidation state but more carbon atoms while the later-generation clusters are the other way around, well following the oxidation trajectory in chemical space.

When considering the characteristics of members in each cluster, we focus solely on high-affiliation species (with a membership degree over 0.5) to simplify the discussion. Figure 8 shows the chemical properties of the high-affiliation species described by their elemental molar ratios and average carbon oxidation state. In general, most of the high-affiliation species of the two early-generation clusters (cluster 1 and 2) center in a relatively low $O_{\text{eff}}:C$ area of the van Krevelen plot, while those from the three later-generation clusters (cluster 3, 4, and 5) spread to the higher $O_{\text{eff}}:C$ area. This confirms that species belonging to later-generation clusters are generally more oxidized than those from early-generation clusters, as expected. With respect to the average oxidation state, species of cluster 1 in general have lower \overline{OS}_C than others, and they are mainly monomers ($n_c = 5$) and dimers ($n_c = 10$). The \overline{OS}_C of species from cluster 2 is slightly higher than that from those of cluster 1, and there are more fragments in this cluster, including both monomers with $n_c < 5$, and dimer species with $5 < n_c < 10$. The high-affiliation species of later-generation clusters generally have higher oxidation degree than that from early-generation clusters, but most of them are molecules with less than 6 carbon atoms.

Formatiert: Einzug: Erste Zeile: 2 Zeich.

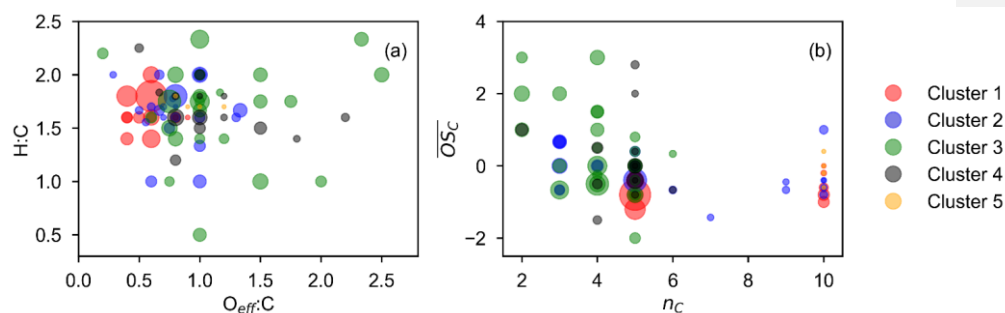


Figure 8. Chemical properties of high-affiliation species from each cluster (with a membership degree larger than 0.5) described by van Krevelen (a) and average carbon oxidation state (\overline{OS}_C) vs. carbon number (n_C) (b) plot. The marker area is proportional to the average signal intensity of species over the whole experiment.

Based on abovementioned results, we conclude that FCM is a feasible dimension-reduction technique for dealing with complex mass spectrometric data from an oxidation system of interest. The derived clusters show a chemical realistic time behavior and cover the major range of chemical properties of the original dataset. This suggests that FCM could be

980 useful in simplification and analyzing mass spectra data and the chemical information
underlying in the clusters ~~and~~ can be helpful to understand the system of interest.

3.3.2 Kinetic properties of different clusters

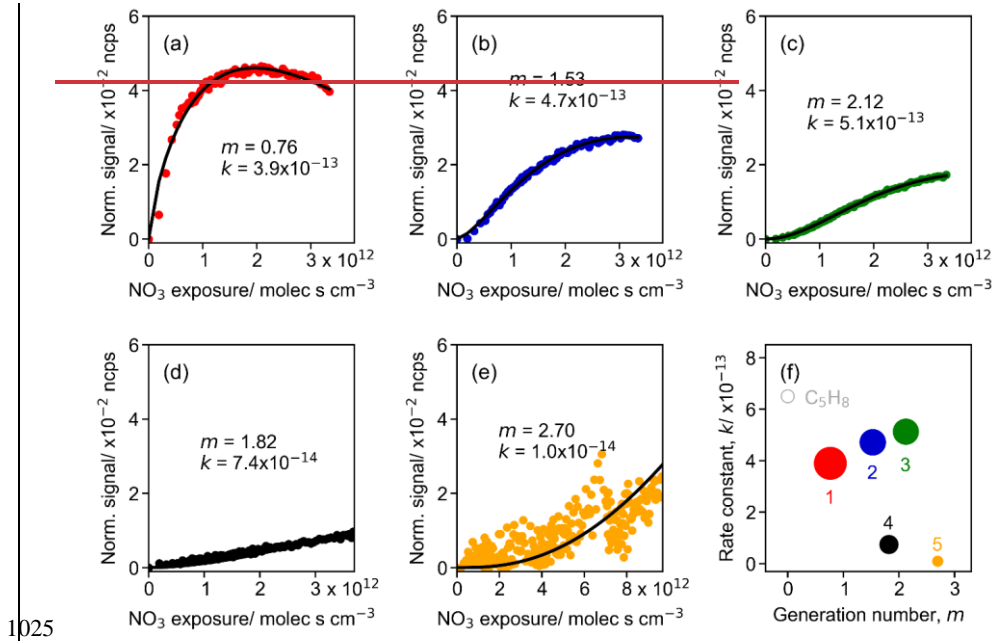
985 ~~Our cluster analysis~~ The FCM results shows that ~~the time series of the cluster centers~~
~~different clusters have different time behaviors,~~ indicating that they ~~are~~-were formed by
different (or a series of) reactions steps. By fitting ~~the measurements to~~ the GKP function (Eq.
12) to the measurements, we can extract underlying kinetic information (effective rate
constant k and generation number $m_{G\#}$) from time series data ~~in terms of exposure to the~~
~~oxidant~~. Generally, a larger value of k implies a faster formation rate of a product class for a
990 given oxidant exposure and vice versa. It should be noted that the k obtained here is not a
stepwise rate constant, and it has no direct relationship to the stepwise rate constants of the
reaction sequence. However, this value offers a way to quantitatively measure the overall rate
constant of all reactions along the pathway (Koss et al., 2020). Since the FCM cluster centers
represent chemically realistic time patterns and ~~thus~~ retain the major ~~chemical-kinetic~~
properties of the original dataset, they can be used as surrogates for various products formed
995 in the isoprene-NO₃ system, and the GKP function can be fitted to the time series of cluster
centers. This largely reduces the complexity of data analysis and provides a way to get kinetic
information directly from measurements.

Figure ~~8-9~~ shows the result of the fit of GKP to the FCM clusters derived from the
chamber measurements for the five-cluster solution. All except cluster 5 fit with a coefficient
1000 of determination (r^2) of 0.96 or higher, indicating that the GKP model can well reproduce the
kinetic behavior of the products formed from the isoprene-NO₃ oxidation system in this study.
Cluster 5 is not well reproduced (with a r^2 of 0.41), probably due to its extremely low and
noisy signal as a surrogate of later-generation products. The fitted values of $m_{G\#}$ for early-
generation clusters are expected to be 1 in theory. As depicted in Fig. ~~8a9a~~, the generation
1005 number of cluster 1 is close to 1, and that of cluster 2 is between 1 and 2, coinciding with the
expectation. As for the three later-generation clusters, their $m_{G\#}$ values are approximately 2
(cluster 3 and 4) or 3 (cluster 5), indicating that they undergo two or more NO₃ oxidation
steps.

There are several possible reasons for non-integer values of $m_{G\#}$, including
1010 uncertainties from signal noise, especially for low signal-to-noise data, and possible
influences from physical processes like vapor-wall interaction, which can lower the signal of
species and thus lead to a higher fitted $m_{G\#}$. (Koss et al., 2020). In addition, the value of

1015 $m_{G\#}$ can be distorted to some extent if compounds are produced from isoprene ~~reactions~~
~~with- oxidation by~~ oxidants other than NO_3 , e.g., OH and O_3 in this case. While NO_3 makes
 up the major fraction of consumption of isoprene ~~and its product, its~~ reactions with O_3 and
 OH still contribute for 10-15% of isoprene loss (Vereecken et al., 2021, Carlson et al., 2022).
 Consequently, it is very likely that some species detected by CIMS were oxidized by multiple
 oxidants. Such an effect will lower $m_{G\#}$ as unaccounted sources increase the concentrations
 of species besides the NO_3 exposure, and the linear, first-order kinetic assumption of the GKP
 1020 model is no longer applicable. For example, the isoprene hydroperoxy aldehyde ($\text{C}_5\text{H}_8\text{O}_3$),
 one of the major products from photooxidation, is also observed from NO_3 -initiated oxidation
 (Vereecken et al., 2021; Wennberg et al., 2018; Wu et al., 2021). Furthermore, the deviation
 of $m_{G\#}$ from integer values can occur if isomers that were formed by a different number of
 oxidation steps exist.

hat formatiert: Schriftart: Nicht Kursiv



1025

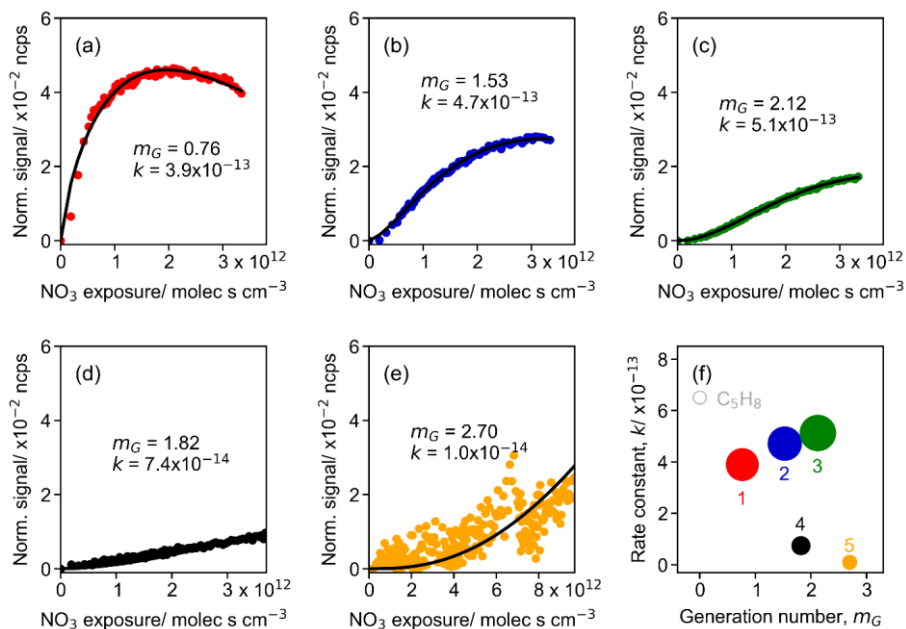


Figure 89. Parameterized effective rate constant (k , $\text{cm}^3 \text{ molecule}^{-1} \text{ s}^{-1}$) and generation number (m_G) for FCM clusters (five-cluster case) derived from CIMS measurements of isoprene-NO₃ system. Panels (a) to (e) show GKP fitting results for different clusters, with cluster 1 in red, cluster 2 in dark blue, cluster 3 in green, cluster 4 in dark, and cluster 5 in orange, respectively. Colored dots in each panel are time series of clusters, and black lines are GKP fits. Panel (f) shows the distribution of kinetic parameters. Marker size/area is proportional to the sum of average intensity of all species in the clusters weighted by their membership degrees.

hat formatiert: Schriftfarbe: Automatisch

hat formatiert: Schriftfarbe: Automatisch

1030

1035

Since the generation number corresponds to the reaction steps with NO₃ to form the product, the later-generation species, which undergo more oxidation steps, should have larger m_G values and higher nitrogen-to-carbon ratios (N:C) when considering only-NO₃ as-is the only oxidant. Figure 9-10 shows the relationship between generation number and chemical properties of clusters. In general, clusters with higher m_G generation numbers have larger N:C ratios, as expected, confirming that NO₃ is the predominate oxidant for isoprene oxidation in our system. Nonetheless, we find that species with larger N:C ratios are not necessarily later-generation products. As shown in Fig. 9a, cluster 4 has a larger N:C ratio than cluster 3 and cluster 5, but it turns out with a smaller m_G , which-This indicates that some of the nitrogen atoms of compounds in cluster 4 were gained through non-oxidative steps. On the other hand, cluster 5 has a larger m_G value than cluster 3 and cluster 4, but its N:C ratio is relatively small. This is likely due to probably because the species in cluster 5 being-were formed by

1040

1045

isoprene oxidation by reactions involving oxidants other than NO_3 , other oxidants than NO_3 , e.g., OH and O_3 . Another plausible explanation could be that the NO_3 oxidation reaction does not lead to an increase in nitrogen content in the product molecules, e.g., through H-abstraction instead of addition to $\text{C}=\text{C}$ double bonds (Wu et al., 2021).

hat formatiert: Tiefgestellt

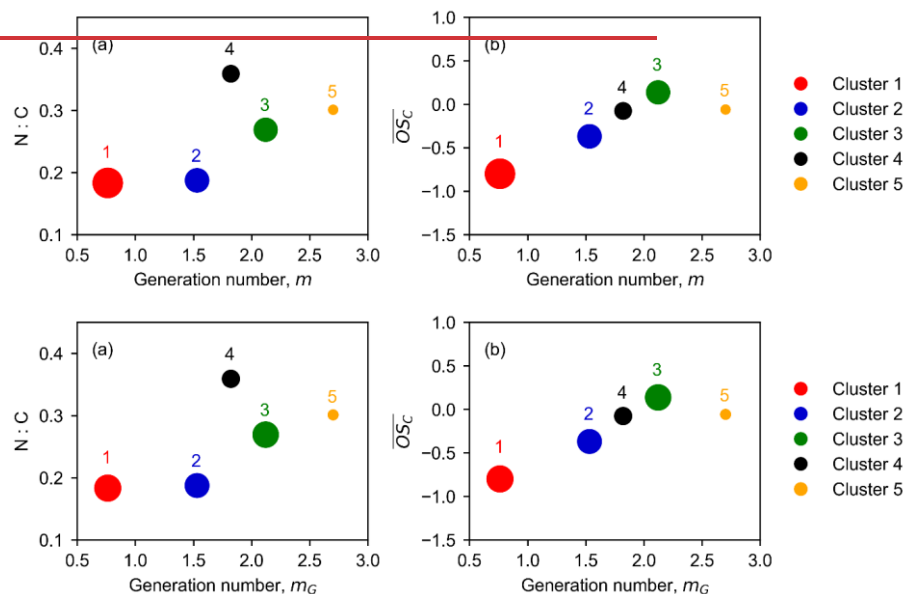


Figure 910. Relationship between generation number (m_G) and chemical properties of clusters: Nitrogen-to-carbon (N:C) ratio (a) and average carbon oxidation state (\overline{OS}_C) (b) as a function of m . The marker size-area is proportional to the square root of the sum of average intensity of all species in the clusters weighted by their membership degrees.

hat formatiert: Schriftfarbe: Automatisch

hat formatiert: Schriftfarbe: Automatisch

There is a strong linear correlation between the generation number and the average oxidation state of the clusters apart from cluster 5, as illustrated in Fig. 9b10b. The early-generation clusters have smaller m_G values than later-generation clusters, which corroborates that the generation number returned by the GKP model is reasonable. The linear regression result shows that the value of \overline{OS}_C increases by ~ 0.74 for each generation. For $m_G = 0$, the corresponding \overline{OS}_C is -1.45 , approximate to the average carbon oxidation state of isoprene ($\overline{OS}_C = -1.6$). For each addition of NO_3 functionality, the \overline{OS}_C of the corresponding product increases by 0.2, and the following O_2 addition (if possible) results in the \overline{OS}_C increasing by additional 0.8. Therefore, it involves at least one autooxidation step for each NO_3 addition considering an increase of about 0.8 in \overline{OS}_C per generation.

Cluster 5 has a $m_{C\#}$ value approaching 3, suggesting that species belonging to this clusters roughly underwent three oxidation steps. However, its average oxidation rate is unexpectedly low, deviating from the linear line of $m_{C\#}$ and \overline{OS}_C . One plausible explanation for this is that such species are probably formed through unimolecular fragmentation. For example, if the H-abstraction (of RO₂) occurs at a carbon with an –OOH functionality attached, the reaction chain will be terminated by OH loss and lead to the formation of a carbonyl formation compound (Bianchi et al., 2019), which results in leads to resulting products with a lower average oxidation state.

In general, the effective rate constants of the clusters are limited by the reaction rate constant of isoprene, and the early-generation clusters have larger k values than the later-generation ones. As shown in Fig. 8f, the returned k values of the two early-generation clusters 1 and 2 are very close to the reaction rate constant of isoprene with NO₃ (6.5×10^{-13} cm³ molecule⁻¹ s⁻¹ at 298K, IUPAC), while those of the later-generation clusters, cluster 4 and 5, are about one order of magnitude smaller. Cluster 3, which represents second-generation products with $m_{C\#} \approx 2$, has a similar effective rate constant as cluster 1 and cluster 2, indicating that the species belonging to this cluster form or react relatively fast. As shown in Fig. 7c, cluster 3 has a high oxidation degree, but less carbon atoms on average, suggesting that the species in cluster 3 are probably highly oxidized fragments. This is confirmed by its mass profile (Fig. 7a).

~~To conclude, the kinetic parameters derived from GKP fitting to the clusters are reasonable and well correlated to the chemical properties of corresponding clusters. Specifically, isoprene products formed in the early stage are larger molecules but less oxidized, with relatively high reactivity, while those formed in the later stage tend to be smaller but highly oxidized with relatively low reactivity. Fragmented species are exceptions that have a relatively high oxidation degree and reactivity simultaneously.~~

3.3.3 Characteristics of members in each cluster

~~Due to the fuzziness of FCM in belongingness of cluster members, only high affiliation species (with a membership degree over 0.5) are considered as members of a cluster in the following discussion for simplicity. Figure 10 shows the chemical properties of the high-affiliation species described by their elemental molar ratios and average carbon oxidation state. In general, most of the high-affiliation species of the two early-generation clusters 1 and 2 fall in the relatively low O:C area of the van Krevelen plot, while those from the three later-generation clusters 3, 4, and 5 are located in the higher O:C range. This confirms that~~

species belonging to later-generation clusters are generally more oxidized than those from early-generation clusters, as expected. With respect to the average oxidation state, species of cluster 1 in general have lower \overline{OS}_c than others, and they are mainly monomers ($n_c = 5$) and dimers ($n_c = 10$). The \overline{OS}_c of species from cluster 2 is slightly higher than that from those of cluster 1, and there are more fragments in this cluster, including both monomers with $n_c < 5$, and dimer species with $5 < n_c < 10$. The high-affiliation species of later-generation clusters generally have higher oxidation degree than that from early-generation clusters, but most of them are molecules with less than 6 carbon atoms.

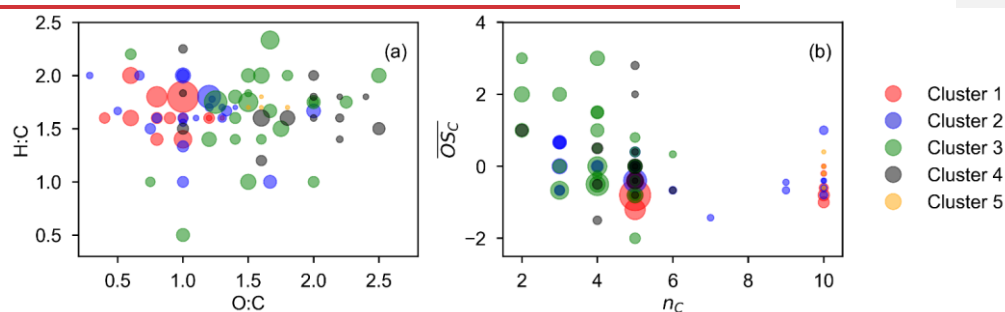


Figure 10. Chemical properties of high-affiliation species from each cluster (with a membership degree larger than 0.5) described by van Krevelen (a) and average carbon oxidation state (\overline{OS}_c) vs. carbon number (n_c) (b) plot. The marker size of species is proportional to the square root of the average signal intensity.

The gamma kinetic parameterization GKP method was also applied to individual species. Examples of fits for various species are shown in Fig. S8. Figure 11 depicts the fitted k and $m_{c\#}$ values of all the high-affiliation species from each cluster. For species from cluster 1, cluster 2, and cluster 3, most of the returned k values fall in the same order of magnitude of 10^{-10} the rate constant of isoprene with NO_3 ($k = 6.5 \times 10^{-13} \text{ cm}^3 \text{ molecule}^{-1} \text{ s}^{-1}$ at 298K). For those from the two later-generation clusters, cluster 4 and 5, the returned k values are about one, respectively, and two order(s) of magnitude smaller, respectively. Most returned $m_{c\#}$ of species from cluster 1 are around 1, indicating that they are formed after one oxidation step (with NO_3), which is consistent with the expectation for early-generation-products. However, the returned $m_{c\#}$ of some species from cluster 1 are between 1 and 2, e.g., the compound(s) with the formula of $\text{C}_5\text{H}_6\text{NO}_5$ (the largest red marker in Fig. 11). This suggests that such species may consist of isomers originating from more than one pathway, with different number of oxidation steps.

For species belonging to cluster 2, their ~~m_G generation numbers~~ are mostly in a range from 1 to 2, but there are also some smaller molecules (mainly C3 and C4 species) with larger ~~m_G generation numbers~~, indicating that such fragmented compounds are formed after multiple oxidation steps. With regard to species from later-generation clusters, the returned ~~m_G~~ values span a broader range, but there are no compounds with a generation number larger than 4. In general, most of the high-affiliation species (from both early- and later-generation) fall in the fast-reacting (large k) area, with a few of exceptions having relatively small although a few can be observed with smaller k and m_G . These two types of compounds are both kinetically realistic. However, there are ~~individual~~ several species with large ~~m_G~~ (around 3) but relatively small k , e.g., $C_{10}H_{17}N_3O_{15}$ and $C_{10}H_{17}N_3O_{16}$ from cluster 5. This suggests that they are slow-forming products that appear after several oxidation steps, which should be difficult to be formed and thus should be low in signal or even undetectable. In fact, the signals of $C_{10}H_{17}N_3O_{15}$ and $C_{10}H_{17}N_3O_{16}$ are extremely low and noisy at the beginning of reaction, as shown in Fig. S8(u) and Fig. S8(v). Detectable increases in signal ~~for of~~ these masses are only observed when the NO_3 exposure ~~is was~~ relatively high.

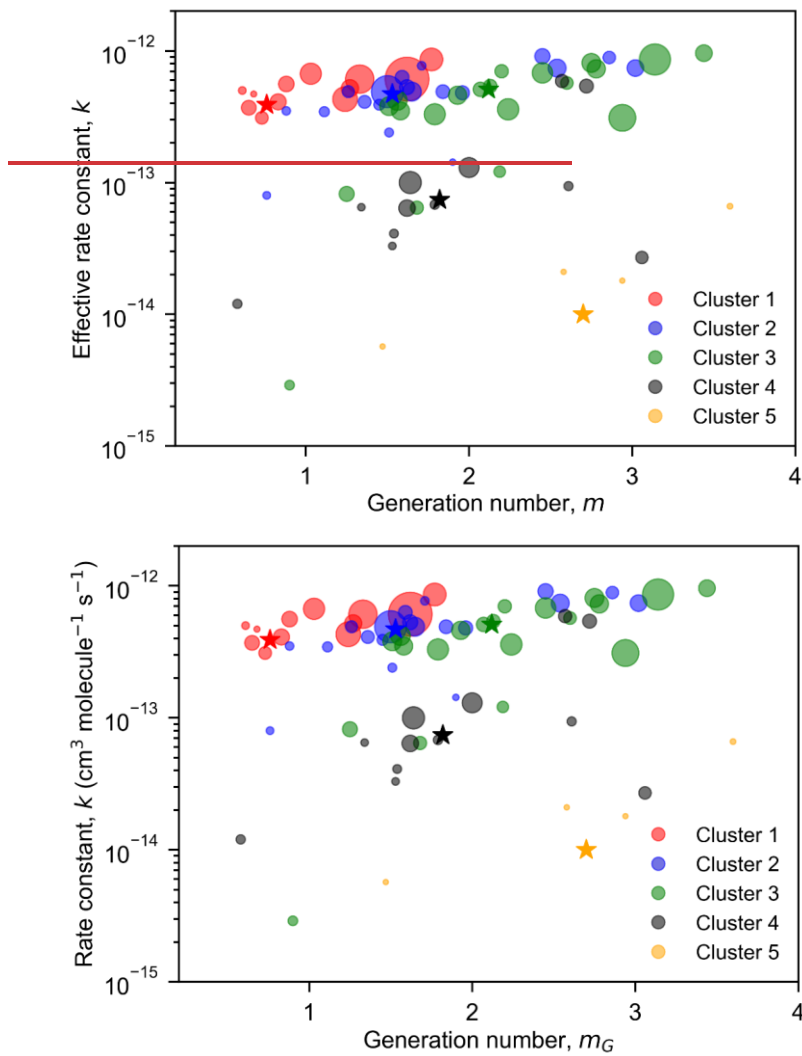


Figure 11. Fitted effective rate constant (k) and generation number (m_G) of the high-affiliation species of each FCM cluster. The cluster centers and members are denoted by color-coded circles and pentagrams, respectively. The marker-circle size-area of individual species is proportional to the square root of the average signal intensity of species over the whole experiment.

To conclude, the kinetic parameters derived from GKP fitting to the clusters are reasonable and well correlated to their chemical properties of corresponding clusters. Specifically, isoprene products formed in the early stage are larger molecules but less oxidized, with relatively high reactivity, while those formed in the later stage tend to be

hat formatiert: Schriftart: Kursiv

hat formatiert: Schriftfarbe: Automatisch

hat formatiert: Schriftfarbe: Automatisch

~~smaller but highly oxidized with relatively low reactivity and less reactive.~~ Fragmented species are exceptions that have a relatively high oxidation degree and reactivity simultaneously.

1155 3.4 Implications to Isoprene-NO₃ chemistry

As noted previously, one big advantage of FCM is that variables can be affiliated to multiple clusters, which relates to many real-world problems in a more realistic and reasonable way. It is elaborated in Sect. 3.3 that different FCM clusters ~~show~~ have distinct differences in chemical and kinetic properties, potentially representing different chemical processes.

1160 Therefore, the clustering distribution of a species ~~can give~~ gives an insight into its formation mechanism.

Figure 12 shows the cluster apportionment of selected major products formed from isoprene oxidation by NO₃. Since ~~each different~~ each FCM clusters represents ~~a different~~ a types of chemical processes or products, ~~that have~~ with distinct chemical and kinetic properties, a different distribution indicates different formation pathways of the respective species. According to the general reaction scheme of isoprene with NO₃ (Scheme S1), 1N- and 2N- monomers are expected to be the first- and second-generation products, respectively. The accretion products are supposed to be formed from RO₂ + RO₂ reaction (Berndt et al., 2018), and thus 2N-dimers are probably originating from self- or cross-reactions of two C5-nitroxy peroxy radicals, while 3N-dimers are most likely produced by cross-reactions of C5-nitroxy peroxy radicals with C5-dinitroxy peroxy radicals (Ng et al., 2008; Wu et al., 2021). According to the general reaction scheme of isoprene with NO₃ (Scheme S1), 1N- and 2N- monomers are expected to be the first- and second-generation products, respectively. The accretion products are supposed to be formed from RO₂ + RO₂ reaction (Berndt et al., 2018), and thus 2N-dimers are probably originating from self- or cross-reactions of two C5-nitroxy peroxy radicals, while 3N-dimers are most likely produced by cross-reactions of C5-nitroxy peroxy radicals with C5-dinitroxy peroxy radicals (Ng et al., 2008; Wu et al., 2021). Accordingly, 2N- and 3N-dimer should be first- and second-generation products, respectively. Possible permutation scheme for the formation of 2N- and 3N-dimers can be found in Table S1 in the supplement.

1175 The FCM results affirm these suppositions to some extent. For example, 1N-monomer species like C₅H₉NO₄ and C₅H₉NO₅ are predominant in early-generation clusters (cluster 1 and cluster 2), while 2N-monomers are mostly found in the later-generation clusters (cluster 3 and cluster 4). However, there are some exceptions, such as C₅H₇NO₆ and C₅H₇NO₇. These two species have entirely different cluster distributions compared to C₅H₇NO₄ and C₅H₇NO₅, regardless of their similar formula composition, ~~and~~ The majority of C₅H₇NO₆ and C₅H₇NO₇ is apportioned to the second-generation cluster (cluster 3). ~~This indicates~~ indicating that C₅H₇NO₆ and C₅H₇NO₇ ~~should bear~~ should bear second-generation products, ~~while whereas~~ C₅H₇NO₄ and C₅H₇NO₅ are subsumed in early-generation products. A similar

1185 phenomenon is observed between $C_5H_9NO_7$ ~~and~~, $C_5H_9NO_{4.5}$, and $C_5H_9NO_5$. Another example is ~~that of~~ the 3N-dimers. ~~By expectation~~In theory, 3N-dimers are supposed to be second-generation products (Table S1), but the FCM outcomes show that different 3N-dimers are formed from different pathways with different generations. For example, $C_{10}H_{17}N_3O_{12}$, $C_{10}H_{17}N_3O_{13}$, and $C_{10}H_{17}N_3O_{14}$ are supposed to be early-generation products based on the FCM results, ~~while-whereas~~ $C_{10}H_{17}N_3O_{15}$ and $C_{10}H_{17}N_3O_{16}$ are ~~supposed formed at a slower rate compared to typical secondary compounds, suggesting them~~ to be third- or even later-generation products ~~that have much lower formation rates compared to typical secondary compounds~~. This implies that the formation mechanisms of 3N-dimers are more complicated than expected. Further investigation is needed to understand distinct behaviors of different 3N-dimers observed in this study.

1195 ~~For~~In terms of 2N-monomers, the clustering results confirm that they are very likely second-generation products, but some species are probably ~~originating-originated~~ from different formation pathways, even though they have the same generation number.

As shown in Fig. 12, most fraction of $C_5H_8N_2O_{8.4}$ and $C_5H_8N_2O_{10}$ fall into cluster 4, ~~while-whereas~~ $C_5H_8N_2O_7$ ~~and~~ $C_5H_{10}N_2O_{8.9}$ and $C_5H_{10}N_2O_9$ are ~~preferably-occupied~~ by ~~primarily assigned to~~ cluster 3. Cluster 3 and cluster 4 are different in chemical and kinetic properties, as ~~noted-described~~ in Sect. 3.3, which most likely representing two different chemical processes. A similar phenomenon is observed ~~for-in~~ $C_{10}H_{16}N_2O_{11}$, which has a distinctive distribution compared to other 2N-dimers. This signifies the uniqueness of its formation mechanism.

1205 Although a species can be apportioned to multiple clusters in FCM, most products in this study predominantly belong to one cluster, e.g., $C_5H_9NO_4$ and $C_5H_9NO_6$, suggesting that they ~~are-dominated~~were formed predominantly through-by a single pathway. In contrast, some species are primarily made up of two clusters, such as $C_5H_7NO_5$, $C_5H_9NO_5$, $C_5H_9NO_7$ and $C_{10}H_{17}N_3O_{12}$, which indicates that they are probably comprised of two structural isomers, or that they originate from two different reaction pathways (with different oxidation steps).

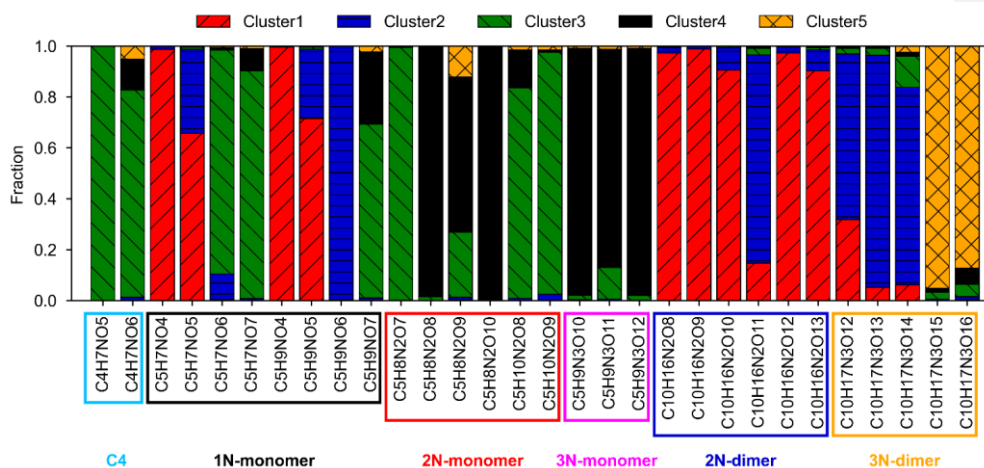


Figure 12. Cluster apportionment of selected major products from the isoprene-NO₃ oxidation system. The colored boxes correspond to different types of products.

1215 All these findings from FCM are useful/valuable and can be used as constraints for mechanism development, especially for less-known species. For example, C₄H₇NO₅ is ubiquitous in the atmosphere and contributes significantly to a C₄ species that contributes a significant fraction of the total isoprene organonitrates, according to our measurements in the SAPHIR chamber, is also ubiquitous in the real atmosphere (Tsiligiannis et al., 2022). However, but it is not well-less investigated (Tsiligiannis et al., 2022), especially its formation mechanism in the nighttime (Tsiligiannis et al., 2022; Wu et al., 2021). Only a few studies mentioned the formation processes of C₄H₇NO₅ in the daytime chemistry (Jenkin et al., 2015; Praske et al., 2015; Schwantes et al., 2015; Wennberg et al., 2018). The formation mechanism of this compound in the nighttime is unclear yet (Tsiligiannis et al., 2022; Wu et al., 2021). According to the FCM outcomes, C₄H₇NO₅ is exclusively assigned to cluster 3 (a second-generation cluster), suggesting that C₄H₇NO₅ is a second-generation product and is mainly originating from one-a single pathway. Combining this information together with its molecular composition, we proposed that C₄H₇NO₅ is potentially-probably formed via further oxidation of the hydroxy carbonyl (C₅H₈O₂) by NO₃, as shown in Scheme S2 in the Supplement (Wu et al., 2021). In a recent publication, Tsiligiannis et al. (2022) have discussed the formation-sources and fate of C₄H₇NO₅ in more detail based on both measurements and modelling results. They suggest that decomposition of C₅H₈NO₇ radicals, nitrated epoxides, or peroxides are also plausible formation pathways for nighttime C₄H₇NO₅. Nonetheless, the fuzzy clustering results in this study suggest that there is only C₄H₇NO₅

~~should be formed only via~~ one major reaction-formation channel (or maybe an unknown pathway) for C₄H₇NO₅ detected in our system~~according to our chamber measurements.~~

4. Conclusions

~~While-~~Recent advances in mass spectrometry, especially the development of CIMS, empowers us to detect low-volatility vapors in the gas phase directly, which-and largely enhances our understanding of the formation mechanism of SOA-~~formation-~~. ~~However,~~ the complex, highly resolved mass spectra introduce new difficulties for data processing and interpreting. Although different statistical analysis techniques, such as PMF, PCA, and HACHCA, were-have been proposed and ~~are~~ widely used to analyze mass spectrometric data, the application of fuzzy clustering algorithms for-in analyzing CIMS data simplification and information extraction has not yet come into common view.

In this study, we promote adopting the FCM method for the analysis of CIMS data obtained from complex oxidation systems. Different from hard clustering algorithms, FCM allows variables to belong to multiple clusters, which is more suitable for overlapping data, and more reasonable for measurements in atmospheric science.

Several parameters need to be defined before running FCM, such as the number of clusters, fuzzifier value, and the distance metric used for measuring dissimilarity, ~~some of which may have an important-critical effect on clustering outcomes including the number of clusters, fuzzifier value, and the distance metric used for measuring dissimilarity.~~ By using multiple clustering validity indices, the effects-impacts of these parameters on partition were evaluated, and their optimal values were determined for our dataset. Furthermore, based on a practical case, we exemplified the functionalities of FCM in understanding the chemical and kinetic properties of the investigated system.

Overall, the FCM approach we presented in this work is an applicable and ~~very~~-useful tool to analyze mass spectrometric data, ~~-~~ which-can-simplify It largely simplifies the characterization of an oxidation system by grouping numerous products into a much smaller number of clusters ~~according to~~based on their different chemical and kinetic properties. The chemical and kinetic information retained from the clustering outcomes helps to understand the chemical processes involved in the investigated system and can be useful for mechanism development.

Data availability

1265 All data given in figures can be displayed in table or in digital form, including those given in
the Supplement. Please send all requests for data to t.mentel@fz-juelich.de and r.wu@fz-juelich.de. The chamber data used in this work are available on the EUROCHAMP database,
(<https://data.eurochamp.org/data-access/chamber-experiments/>, EUROCHAMP, 2020) under
<https://doi.org/10.25326/JTYK-5V47> (Fuchs et al., 2020).

1270 Competing interests

The authors declare that they have no conflict of interest.

Author contributions

TFM and SRZ designed the study. RW and SK collected CIMS data, and RW did the data
analysis. RW and TFM wrote the paper. All co-authors discussed the results and commented
1275 on the paper.

Acknowledgement

This work has received funding from the European Research Council (ERC) and European
Commission (EC) under the European Union's Horizon 2020 research and innovation
program (SARLEP grant agreement No. 681529, and Eurochamp 2020 grant agreement No.
1280 730997). The personnel of the ISOPNO₃ campaign are acknowledged for the help during the
campaign.

FORCES!

References

- 1285 Äijälä, M., Heikkinen, L., Fröhlich, R., Canonaco, F., Prévôt, A. S., Junninen, H., Petäjä, T.,
Kulmala, M., Worsnop, D., and Ehn, M.: Resolving anthropogenic aerosol pollution types–
deconvolution and exploratory classification of pollution events, *Atmospheric Chemistry
and Physics*, 17, 3165-3197, 2017.
- Albrecht, S. R., Novelli, A., Hofzumahaus, A., Kang, S., Baker, Y., Mentel, T., Wahner, A.,
1290 and Fuchs, H.: Measurements of hydroperoxy radicals (HO₂) at atmospheric
concentrations using bromide chemical ionisation mass spectrometry, *Atmospheric
Measurement Techniques*, 12, 891-902, 10.5194/amt-12-891-2019, 2019.
- Arora, J., Khatter, K., and Tushir, M.: Fuzzy c-means clustering strategies: A review of
distance measures, *Software Engineering*, 153-162, 2019.
- 1295 Berndt, T., Scholz, W., Mentler, B., Fischer, L., Herrmann, H., Kulmala, M., and Hansel, A.:
Accretion Product Formation from Self- and Cross-Reactions of RO₂ Radicals in the
Atmosphere, *Angew Chem Int Ed Engl*, 57, 3820-3824, 10.1002/anie.201710989, 2018.
- Bezdek, J. C. and Pal, N. R.: Some new indexes of cluster validity, *IEEE Transactions on
Systems, Man, and Cybernetics, Part B (Cybernetics)*, 28, 301-315, 1998.
- 1300 Bezdek, J. C., Ehrlich, R., and Full, W.: FCM: The fuzzy c-means clustering algorithm,
Computers & geosciences, 10, 191-203, 1984.
- Bianchi, F., Kurten, T., Riva, M., Mohr, C., Rissanen, M. P., Roldin, P., Berndt, T., Crouse,
J. D., Wennberg, P. O., Mentel, T. F., Wildt, J., Junninen, H., Jokinen, T., Kulmala, M.,
Worsnop, D. R., Thornton, J. A., Donahue, N., Kjaergaard, H. G., and Ehn, M.: Highly
1305 Oxygenated Organic Molecules (HOM) from Gas-Phase Autoxidation Involving Peroxy
Radicals: A Key Contributor to Atmospheric Aerosol, *Chem Rev*, 119, 3472-3509,
10.1021/acs.chemrev.8b00395, 2019.
- Bouguessa, M. and Wang, S.-R.: A new efficient validity index for fuzzy clustering,
Proceedings of 2004 International Conference on Machine Learning and Cybernetics
1310 (IEEE Cat. No. 04EX826), 1914-1919, 2004.
- Bouguessa, M., Wang, S., and Sun, H.: An objective approach to cluster validation, *Pattern
Recognition Letters*, 27, 1419-1430, 10.1016/j.patrec.2006.01.015, 2006.
- Bozzetti, C., El Haddad, I., Salameh, D., Daellenbach, K. R., Fermo, P., Gonzalez, R.,
Minguillón, M. C., Iinuma, Y., Poulain, L., and Elser, M.: Organic aerosol source

- 1315 apportionment by offline-AMS over a full year in Marseille, *Atmospheric Chemistry and Physics*, 17, 8247-8268, 2017.
- Breitenlechner, M., Fischer, L., Hainer, M., Heinritzi, M., Curtius, J., and Hansel, A.: PTR3: an instrument for studying the lifecycle of reactive organic carbon in the atmosphere, *Analytical chemistry*, 89, 5824-5831, 2017.
- 1320 Brown, S. G., Frankel, A., and Hafner, H. R.: Source apportionment of VOCs in the Los Angeles area using positive matrix factorization, *Atmospheric Environment*, 41, 227-237, 2007.
- [Buchholz, A., Ylisirniö, A., Huang, W., Mohr, C., Canagaratna, M., Worsnop, D. R., Schobesberger, S., and Virtanen, A.: Deconvolution of FIGAERO-CIMS thermal desorption profiles using positive matrix factorisation to identify chemical and physical processes during particle evaporation, *Atmos. Chem. Phys.*, 20, 7693-7716, <https://doi.org/10.5194/acp-20-7693-2020>, 2020.](https://doi.org/10.5194/acp-20-7693-2020)
- ~~[Buchholz, A., Lambe, A. T., Ylisirniö, A., Li, Z., Tikkanen, O. P., Faiola, C., Kari, E., Hao, L., Luoma, O., Huang, W., Mohr, C., Worsnop, D. R., Nizkorodov, S. A., Yli Juuti, T., Schobesberger, S., and Virtanen, A.: Insights into the O  C-dependent mechanisms controlling the evaporation of <i></i>pinene secondary organic aerosol particles, *Atmospheric Chemistry and Physics*, 19, 4061-4073, \[10.5194/acp-19-4061-2019\]\(https://doi.org/10.5194/acp-19-4061-2019\), 2019.](https://doi.org/10.5194/acp-19-4061-2019)~~
- Campello, R. J. G. B. and Hruschka, E. R.: A fuzzy extension of the silhouette width criterion for cluster analysis, *Fuzzy Sets and Systems*, 157, 2858-2875, [10.1016/j.fss.2006.07.006](https://doi.org/10.1016/j.fss.2006.07.006), 2006.
- 1335 Canonaco, F., Crippa, M., Slowik, J. G., Baltensperger, U., and Prévôt, A. S.: SoFi, an IGOR-based interface for the efficient use of the generalized multilinear engine (ME-2) for the source apportionment: ME-2 application to aerosol mass spectrometer data, *Atmospheric Measurement Techniques*, 6, 3649-3661, 2013.
- 1340 Carlsson, P., Vereecken, L., Novelli, A., Bernard, F., Brown, S. S., Brownwood, B., Cho, C., Crowley, J. N., Dewald, P., and Edwards, P. M.: Comparison of isoprene chemical mechanisms at atmospheric night-time conditions in chamber experiments: Evidence of hydroperoxy aldehydes and epoxy products from NO₃ oxidation, *EGUsphere*, 1-50, 2022.
- [Carlton, A. G., Wiedinmyer, C., and Kroll, J. H.: A review of Secondary Organic Aerosol \(SOA\) formation from isoprene, *Atmos. Chem. Phys.*, 9, 4987-5005, \[10.5194/acp-9-4987-2009\]\(https://doi.org/10.5194/acp-9-4987-2009\), 2009.](https://doi.org/10.5194/acp-9-4987-2009)

- 1350 Chen, H.-y., Teng, Y.-g., Wang, J.-s., Song, L.-t., and Zuo, R.: Source apportionment of sediment PAHs in the Pearl River Delta region (China) using nonnegative matrix factorization analysis with effective weighted variance solution, *Science of the total environment*, 444, 401-408, 2013.
- [Chen, L.-W. A., Watson, J. G., Chow, J. C., DuBois, D. W., and Herschberger, L.: PM2.5 source apportionment: reconciling receptor models for US nonurban and urban long-term networks, *Journal of the Air & Waste Management Association*, 61, 1204-1217, 2011.](#)
- 1355 Chhabra, P., Ng, N., Canagaratna, M., Corrigan, A., Russell, L., Worsnop, D., Flagan, R., and Seinfeld, J.: Elemental composition and oxidation of chamber organic aerosol, *Atmospheric Chemistry and Physics*, 11, 8827-8845, 2011.
- Crouse, J. D., Nielsen, L. B., Jørgensen, S., Kjaergaard, H. G., and Wennberg, P. O.: Autoxidation of Organic Compounds in the Atmosphere, *The Journal of Physical Chemistry Letters*, 4, 3513-3520, 10.1021/jz4019207, 2013.
- 1360 Devarajan, K.: Nonnegative matrix factorization: an analytical and interpretive tool in computational biology, *PLoS computational biology*, 4, e1000029, 2008.
- Dik, A., Bouroumi, A., and Ettouhami, A.: Weighted distances for fuzzy clustering, *Applied Mathematical Sciences*, 8, 147-156, 2014.
- 1365 Donahue, N. M., Kroll, J. H., Pandis, S. N., and Robinson, A. L.: A two-dimensional volatility basis set – Part 2: Diagnostics of organic-aerosol evolution, *Atmos. Chem. Phys.*, 12, 615-634, 2012.
- Ehn, M., Kleist, E., Junninen, H., Petäjä, T., Lönn, G., Schobesberger, S., Dal Maso, M., Trimborn, A., Kulmala, M., Worsnop, D. R., Wahner, A., Wildt, J., and Mentel, T. F.: Gas phase formation of extremely oxidized pinene reaction products in chamber and ambient air, *Atmospheric Chemistry and Physics*, 12, 5113-5127, 10.5194/acp-12-5113-2012, 2012.
- 1370 Ehn, M., Thornton, J. A., Kleist, E., Sipila, M., Junninen, H., Pullinen, I., Springer, M., Rubach, F., Tillmann, R., Lee, B., Lopez-Hilfiker, F., Andres, S., Acir, I. H., Rissanen, M., Jokinen, T., Schobesberger, S., Kangasluoma, J., Kontkanen, J., Nieminen, T., Kurten, T., Nielsen, L. B., Jørgensen, S., Kjaergaard, H. G., Canagaratna, M., Maso, M. D., Berndt, T., Petaja, T., Wahner, A., Kerminen, V. M., Kulmala, M., Worsnop, D. R., Wildt, J., and Mentel, T. F.: A large source of low-volatility secondary organic aerosol, *Nature*, 506, 476-479, 10.1038/nature13032, 2014.
- [Fry, J. L., Brown, S. S., Middlebrook, A. M., Edwards, P. M., Campuzano-Jost, P., Day, D. A., Jimenez, J. L., Allen, H. M., Ryerson, T. B., Pollack, I., Graus, M., Warneke, C., de Gouw, J. A., Brock, C. A., Gilman, J., Lerner, B. M., Dubé, W. P., Liao, J., and Welti, A.:](#)
- 1380

[Secondary organic aerosol \(SOA\) yields from NO₃ radical + isoprene based on nighttime aircraft power plant plume transects, Atmos. Chem. Phys., 18, 11663-11682, 10.5194/acp-18-11663-2018, 2018.](#)

- 1385 Fu, X., Huang, K., Sidiropoulos, N. D., and Ma, W.-K.: Nonnegative matrix factorization for signal and data analytics: Identifiability, algorithms, and applications, *IEEE Signal Process. Mag.*, 36, 59-80, 2019.
- Fukuyama, Y.: A new method of choosing the number of clusters for the fuzzy c-mean method, *Proc. 5th Fuzzy Syst. Symp.*, 1989, 247-250.
- 1390 Gao, X.-B., PEI, J.-h., and XIE, W.-x.: A study of weighting exponent m in a fuzzy c-means algorithm, *ACTA ELECTONICA SINICA*, 28, 80, 2000.
- Gath, I. and Geva, A. B.: Unsupervised optimal fuzzy clustering, *IEEE Transactions on pattern analysis and machine intelligence*, 11, 773-780, 1989.
- Ghosh, S. and Dubey, S. K.: Comparative analysis of k-means and fuzzy c-means algorithms, 1395 *International Journal of Advanced Computer Science and Applications*, 4, 2013.
- Gueorguieva, N., Valova, I., and Georgiev, G.: M&MFCM: fuzzy c-means clustering with mahalanobis and minkowski distance metrics, *Procedia computer science*, 114, 224-233, 2017.
- Hallquist, M., Wenger, J., Baltensperger, U., Rudich, Y., Simpson, D., Claeys, M., Dommen, 1400 J., Donahue, N., George, C., and Goldstein, A.: The formation, properties and impact of secondary organic aerosol: current and emerging issues, *Atmospheric Chemistry and Physics*, 9, 5155-5236, 2009.
- Hammah, R. and Curran, J.: Fuzzy cluster algorithm for the automatic identification of joint sets, *International Journal of Rock Mechanics and Mining Sciences*, 35, 889-905, 1998.
- 1405 Haqiqi, B. N. and Kurniawan, R.: Analisis Perbandingan Metode Fuzzy C-Means Dan Subtractive Fuzzy C-Means, *Media Statistika*, 8, 59-67, 2015.
- Hastie, T., Tibshirani, R., Friedman, J. H., and Friedman, J. H.: *The elements of statistical learning: data mining, inference, and prediction*, Springer 2009.
- Hathaway, R. J. and Bezdek, J. C.: Fuzzy c-means clustering of incomplete data, 1410 *IEEE Transactions on Systems, Man, and Cybernetics, Part B (Cybernetics)*, 31, 735-744, 2001.
- Heikkinen, L., Äijälä, M., Daellenbach, K. R., Chen, G., Garmash, O., Aliaga, D., Graeffe, F., Rätty, M., Luoma, K., and Aalto, P.: Eight years of sub-micrometre organic aerosol composition data from the boreal forest characterized using a machine-learning approach, *Atmospheric Chemistry and Physics*, 21, 10081-10109, 2021.

- 1415 Huang, M., Xia, Z., Wang, H., Zeng, Q., and Wang, Q.: The range of the value for the fuzzifier of the fuzzy c-means algorithm, *Pattern Recognition Letters*, 33, 2280-2284, 2012.
- Hwang, C. and Rhee, F. C.-H.: Uncertain fuzzy clustering: Interval type-2 fuzzy approach to $\$c\$$ means, *IEEE Transactions on fuzzy systems*, 15, 107-120, 2007.
- Jenkin, M. E., Young, J. C., and Rickard, A. R.: The MCM v3.3.1 degradation scheme for isoprene, *Atmospheric Chemistry and Physics*, 15, 11433-11459, 10.5194/acp-15-11433-2015, 2015.
- 1420 Jimenez, J. L., Canagaratna, M., Donahue, N., Prevot, A., Zhang, Q., Kroll, J. H., DeCarlo, P. F., Allan, J. D., Coe, H., and Ng, N.: Evolution of organic aerosols in the atmosphere, *science*, 326, 1525-1529, 2009.
- 1425 Jokinen, T., Berndt, T., Makkonen, R., Kerminen, V. M., Junninen, H., Paasonen, P., Stratmann, F., Herrmann, H., Guenther, A. B., Worsnop, D. R., Kulmala, M., Ehn, M., and Sipila, M.: Production of extremely low volatile organic compounds from biogenic emissions: Measured yields and atmospheric implications, *Proc Natl Acad Sci U S A*, 112, 7123-7128, 10.1073/pnas.1423977112, 2015.
- 1430 Karl, T., Striednig, M., Graus, M., Hammerle, A., and Wohlfahrt, G.: Urban flux measurements reveal a large pool of oxygenated volatile organic compound emissions, *Proceedings of the National Academy of Sciences*, 115, 1186-1191, 2018.
- Kaufman, L. and Rousseeuw, P. J.: *Finding groups in data: an introduction to cluster analysis*, John Wiley & Sons 2009.
- 1435 Kirkby, J., Duplissy, J., Sengupta, K., Frege, C., Gordon, H., Williamson, C., Heinritzi, M., Simon, M., Yan, C., Almeida, J., Trostl, J., Nieminen, T., Ortega, I. K., Wagner, R., Adamov, A., Amorim, A., Bernhammer, A. K., Bianchi, F., Breitenlechner, M., Brilke, S., Chen, X., Craven, J., Dias, A., Ehrhart, S., Flagan, R. C., Franchin, A., Fuchs, C., Guida, R., Hakala, J., Hoyle, C. R., Jokinen, T., Junninen, H., Kangasluoma, J., Kim, J., Krapf, M.,
- 1440 Kurten, A., Laaksonen, A., Lehtipalo, K., Makhmutov, V., Mathot, S., Molteni, U., Onnela, A., Perakyla, O., Piel, F., Petaja, T., Praplan, A. P., Pringle, K., Rap, A., Richards, N. A., Riipinen, I., Rissanen, M. P., Rondo, L., Sarnela, N., Schobesberger, S., Scott, C. E., Seinfeld, J. H., Sipila, M., Steiner, G., Stozhkov, Y., Stratmann, F., Tome, A., Virtanen, A., Vogel, A. L., Wagner, A. C., Wagner, P. E., Weingartner, E., Wimmer, D., Winkler, P. M.,
- 1445 Ye, P., Zhang, X., Hansel, A., Dommen, J., Donahue, N. M., Worsnop, D. R., Baltensperger, U., Kulmala, M., Carslaw, K. S., and Curtius, J.: Ion-induced nucleation of pure biogenic particles, *Nature*, 533, 521-526, 10.1038/nature17953, 2016.

- 1450 Koss, A. R., Canagaratna, M. R., Zaytsev, A., Krechmer, J. E., Breitenlechner, M., Nihill, K. J., Lim, C. Y., Rowe, J. C., Roscioli, J. R., and Keutsch, F. N.: Dimensionality-reduction techniques for complex mass spectrometric datasets: application to laboratory atmospheric organic oxidation experiments, *Atmospheric chemistry and physics*, 20, 1021-1041, 2020.
- Krechmer, J., Lopez-Hilfiker, F., Koss, A., Hutterli, M., Stoerner, C., Deming, B., Kimmel, J., Warneke, C., Holzinger, R., Jayne, J., Worsnop, D., Fuhrer, K., Gonin, M., and de Gouw, J.: Evaluation of a New Reagent-Ion Source and Focusing Ion-Molecule Reactor for Use in Proton-Transfer-Reaction Mass Spectrometry, *Anal Chem*, 90, 12011-12018, 10.1021/acs.analchem.8b02641, 2018.
- 1455 [Kroll, J. H., Ng, N. L., Murphy, S. M., Flagan, R. C., and Seinfeld, J. H.: Secondary organic aerosol formation from isoprene photooxidation, *Environ. Sci. Technol.*, 40, 1869–1877, <https://doi.org/10.1021/es0524301>, 2006.](https://doi.org/10.1021/es0524301)
- 1460 Kryszczuk, K. and Hurley, P.: Estimation of the number of clusters using multiple clustering validity indices, *International workshop on multiple classifier systems*, 114-123,
- Kwon, S.-H.: Cluster validity index for fuzzy clustering, *Electronics Letters*, 34, 2176-2177, 1998.
- Kwon, S. H., Kim, J., and Son, S. H.: Improved cluster validity index for fuzzy clustering, *Electronics Letters*, 57, 792-794, 2021.
- 1465 Lanz, V., Alfarra, M., Baltensperger, U., Buchmann, B., Hueglin, C., and Prévôt, A.: Source apportionment of submicron organic aerosols at an urban site by factor analytical modelling of aerosol mass spectra, *Atmospheric Chemistry and Physics*, 7, 1503-1522, 2007.
- 1470 Lanz, V. A., Henne, S., Staehelin, J., Hueglin, C., Vollmer, M. K., Steinbacher, M., Buchmann, B., and Reimann, S.: Statistical analysis of anthropogenic non-methane VOC variability at a European background location (Jungfraujoch, Switzerland), *Atmospheric Chemistry and Physics*, 9, 3445-3459, 2009.
- 1475 Lanz, V. A., Alfarra, M. R., Baltensperger, U., Buchmann, B., Hueglin, C., Szidat, S., Wehrli, M. N., Wacker, L., Weimer, S., and Caseiro, A.: Source attribution of submicron organic aerosols during wintertime inversions by advanced factor analysis of aerosol mass spectra, *Environmental science & technology*, 42, 214-220, 2008.
- Lee, D. D. and Seung, H. S.: Learning the parts of objects by non-negative matrix factorization, *Nature*, 401, 788-791, 1999.
- 1480 Li, H., Canagaratna, M. R., Riva, M., Rantala, P., Zhang, Y., Thomas, S., Heikkinen, L., Flaud, P.-M., Villenave, E., and Perraudin, E.: Atmospheric organic vapors in two

- European pine forests measured by a Vocus PTR-TOF: insights into monoterpene and sesquiterpene oxidation processes, *Atmospheric Chemistry and Physics*, 21, 4123-4147, 2021.
- 1485 Li, Z., D'Ambro, E. L., Schobesberger, S., Gaston, C. J., Lopez-Hilfiker, F. D., Liu, J., Shilling, J. E., Thornton, J. A., and Cappa, C. D.: A robust clustering algorithm for analysis of composition-dependent organic aerosol thermal desorption measurements, *Atmospheric Chemistry and Physics*, 20, 2489-2512, 2020.
- Malley, C. S., Braban, C. F., and Heal, M. R.: The application of hierarchical cluster analysis and non-negative matrix factorization to European atmospheric monitoring site classification, *Atmospheric research*, 138, 30-40, 2014.
- 1490 Ng, N., Kwan, A., Surratt, J., Chan, A., Chhabra, P., Sorooshian, A., Pye, H. O., Crounse, J., Wennberg, P., and Flagan, R.: Secondary organic aerosol (SOA) formation from reaction of isoprene with nitrate radicals (NO₃), *Atmospheric Chemistry and Physics*, 8, 4117-4140, 2008.
- 1495 Nishom, M.: Perbandingan Akurasi Euclidean Distance, Minkowski Distance, dan Manhattan Distance pada Algoritma K-Means Clustering berbasis Chi-Square, *Jurnal Informatika*, 4, 20-24, 2019.
- Ozkan, I. and Turksen, I.: Upper and lower values for the level of fuzziness in FCM, in: *Fuzzy Logic*, Springer, 99-112, 2007.
- 1500 Paatero, P.: Least squares formulation of robust non-negative factor analysis, *Chemometrics and intelligent laboratory systems*, 37, 23-35, 1997.
- Paatero, P. and Tapper, U.: Positive matrix factorization: A non - negative factor model with optimal utilization of error estimates of data values, *Environmetrics*, 5, 111-126, 1994.
- 1505 ~~Paatero, P., Eberly, S., Brown, S., and Norris, G.: Methods for estimating uncertainty in factor analytic solutions, *Atmospheric Measurement Techniques*, 7, 781-797, 2014.~~
- Pal, N. R. and Bezdek, J. C.: On cluster validity for the fuzzy c-means model, *IEEE Transactions on Fuzzy systems*, 3, 370-379, 1995.
- Pöschl, U.: Atmospheric aerosols: composition, transformation, climate and health effects, *Angewandte Chemie International Edition*, 44, 7520-7540, 2005.
- 1510 Praske, E., Crounse, J. D., Bates, K. H., Kurtén, T., Kjaergaard, H. G., and Wennberg, P. O.: Atmospheric fate of methyl vinyl ketone: Peroxy radical reactions with NO and HO₂, *The Journal of Physical Chemistry A*, 119, 4562-4572, 2015.

- 1515 Praske, E., Otkjær, R. V., Crounse, J. D., Hethcox, J. C., Stoltz, B. M., Kjaergaard, H. G., and Wennberg, P. O.: Atmospheric autoxidation is increasingly important in urban and suburban North America, *Proceedings of the National Academy of Sciences*, 115, 64-69, 2018.
- 1520 Priestley, M., Bannan, T. J., Le Breton, M., Worrall, S. D., Kang, S., Pullinen, I., Schmitt, S., Tillmann, R., Kleist, E., Zhao, D., Wildt, J., Garmash, O., Mehra, A., Bacak, A., Shallcross, D. E., Kiendler-Scharr, A., Hallquist, Å. M., Ehn, M., Coe, H., Percival, C. J., Hallquist, M., Mentel, T. F., and McFiggans, G.: Chemical characterisation of benzene oxidation products under high- and low-NO_x conditions using chemical ionisation mass spectrometry, *Atmospheric Chemistry and Physics*, 21, 3473-3490, 10.5194/acp-21-3473-2021, 2021.
- 1525 Pullinen, I., Schmitt, S., Kang, S., Sarrafzadeh, M., Schlag, P., Andres, S., Kleist, E., Mentel, T. F., Rohrer, F., and Springer, M.: Impact of NO_x on secondary organic aerosol (SOA) formation from α -pinene and β -pinene photooxidation: the role of highly oxygenated organic nitrates, *Atmospheric chemistry and physics*, 20, 10125-10147, 2020.
- 1530 Rawashdeh, M. and Ralescu, A. L.: Fuzzy Cluster Validity with Generalized Silhouettes, [Midwest Artificial Intelligence and Cognitive Science Conference, MAICS, 2012.](#)
- [Reff, A., Eberly, S. I., and Bhave, P. V.: Receptor modeling of ambient particulate matter data using positive matrix factorization: review of existing methods, *Journal of the Air & Waste Management Association*, 57, 146-154, 2007.](#)
- 1535 Ren, M., Liu, P., Wang, Z., and Yi, J.: A self-adaptive fuzzy c-means algorithm for determining the optimal number of clusters, *Computational intelligence and neuroscience*, 2016, 2016.
- Rohrer, F., Bohn, B., Brauers, T., Brüning, D., Johnen, F. J., Wahner, A., and Kleffmann, J.: Characterisation of the photolytic HONO-source in the atmosphere simulation chamber SAPHIR, *Atmospheric Chemistry and Physics*, 5, 2189-2201, 10.5194/acp-5-2189-2005, 2005.
- 1540 [Rollins, A. W., Kiendler-Scharr, A., Fry, J., Brauers, T., Brown, S. S., Dorn, H.-P., Dubé, W. P., Fuchs, H., Mensah, A., and Mentel, T.: Isoprene oxidation by nitrate radical: alkyl nitrate and secondary organic aerosol yields, *Atmos. Chem. Phys.*, 9, 6685-6703, 10.5194/acp-9-6685-2009, 2009.](#)
- 1545 Rosati, B., Teiwes, R., Kristensen, K., Bossi, R., Skov, H., Glasius, M., Pedersen, H. B., and Bilde, M.: Factor analysis of chemical ionization experiments: Numerical simulations and

- an experimental case study of the ozonolysis of α -pinene using a PTR-ToF-MS, *Atmospheric Environment*, 199, 15-31, 2019.
- Rousseeuw, P. J.: Silhouettes: a graphical aid to the interpretation and validation of cluster analysis, *Journal of computational and applied mathematics*, 20, 53-65, 1987
- 1550 Schwämmle, V. and Jensen, O. N.: A simple and fast method to determine the parameters for fuzzy c-means cluster analysis, *Bioinformatics*, 26, 2841-2848, 2010.
- Schwantes, R. H., Teng, A. P., Nguyen, T. B., Coggon, M. M., Crouse, J. D., St Clair, J. M., Zhang, X., Schilling, K. A., Seinfeld, J. H., and Wennberg, P. O.: Isoprene NO₃ Oxidation Products from the RO₂ + HO₂ Pathway, *J Phys Chem A*, 119, 10158-10171, 10.1021/acs.jpca.5b06355, 2015.
- 1555 Shrivastava, M., Cappa, C. D., Fan, J., Goldstein, A. H., Guenther, A. B., Jimenez, J. L., Kuang, C., Laskin, A., Martin, S. T., Ng, N. L., Petaja, T., Pierce, J. R., Rasch, P. J., Roldin, P., Seinfeld, J. H., Shilling, J., Smith, J. N., Thornton, J. A., Volkamer, R., Wang, J., Worsnop, D. R., Zaveri, R. A., Zelenyuk, A., and Zhang, Q.: Recent advances in understanding secondary organic aerosol: Implications for global climate forcing, *Reviews of Geophysics*, 55, 509-559, 10.1002/2016rg000540, 2017.
- 1560 Simovici, D. A. and Jaroszewicz, S.: An axiomatization of partition entropy, *IEEE Transactions on Information Theory*, 48, 2138-2142, 2002.
- 1565 Singh, A., Agarwal, J., and Rana, A.: Performance measure of similis and fp-growth algorithm, *International Journal of Computer Applications*, 62, 2013.
- Sofowote, U. M., McCarry, B. E., and Marvin, C. H.: Source apportionment of PAH in Hamilton Harbour suspended sediments: comparison of two factor analysis methods, *Environmental science & technology*, 42, 6007-6014, 2008.
- 1570 Song, K., Guo, S., Wang, H., Yu, Y., Wang, H., Tang, R., Xia, S., Gong, Y., Wan, Z., and Lv, D.: Measurement report: Online measurement of gas-phase nitrated phenols utilizing a CI-LToF-MS: primary sources and secondary formation, *Atmospheric Chemistry and Physics*, 21, 7917-7932, 2021.
- 1575 Spracklen, D., Jimenez, J., Carslaw, K., Worsnop, D., Evans, M., Mann, G., Zhang, Q., Canagaratna, M., Allan, J., and Coe, H.: Aerosol mass spectrometer constraint on the global secondary organic aerosol budget, *Atmospheric Chemistry and Physics*, 11, 12109-12136, 2011.
- 1580 Stark, H., Yatavelli, R. L. N., Thompson, S. L., Kimmel, J. R., Cubison, M. J., Chhabra, P. S., Canagaratna, M. R., Jayne, J. T., Worsnop, D. R., and Jimenez, J. L.: Methods to extract molecular and bulk chemical information from series of complex mass spectra with limited

- mass resolution, *International Journal of Mass Spectrometry*, 389, 26-38, 10.1016/j.ijms.2015.08.011, 2015.
- Subbalakshmi, C., Krishna, G. R., Rao, S. K. M., and Rao, P. V.: A method to find optimum number of clusters based on fuzzy silhouette on dynamic data set, *Procedia Computer Science*, 46, 346-353, 2015.
- 1585 [Surratt, J. D., Lin, Y.-H., Arashiro, M., Vizuete, W. G., Zhang, Z., Gold, A., Jaspers, I., and Fry, R. C.: Understanding the early biological effects of isoprene-derived particulate matter enhanced by anthropogenic pollutants, Research Reports: Health Effects Institute, 2019, 2019.](#)
- 1590 Tsiligiannis, E., Wu, R., Lee, B. H., Salvador, C. M., Priestley, M., Carlsson, P. T., Kang, S., Novelli, A., Vereecken, L., and Fuchs, H.: A four carbon organonitrate as a significant product of secondary isoprene chemistry, *Geophysical research letters*, 49, e2021GL097366, 2022.
- Ulbrich, I., Canagaratna, M., Zhang, Q., Worsnop, D., and Jimenez, J.: Interpretation of 1595 organic components from Positive Matrix Factorization of aerosol mass spectrometric data, *Atmospheric Chemistry and Physics*, 9, 2891-2918, 2009.
- Vélez-Falconí, M., Marín, J., Jiménez, S., and Guachi-Guachi, L.: Comparative Study of Distance Measures for the Fuzzy C-means and K-means Non-Supervised Methods Applied to Image Segmentation, *ICAI Workshops*, 1-14,
- 1600 Vereecken, L., Carlsson, P., Novelli, A., Bernard, F., Brown, S., Cho, C., Crowley, J., Fuchs, H., Mellouki, W., and Reimer, D.: Theoretical and experimental study of peroxy and alkoxy radicals in the NO₃-initiated oxidation of isoprene, *Physical Chemistry Chemical Physics*, 23, 5496-5515, 2021.
- Vlasenko, A., Slowik, J., Bottenheim, J., Brickell, P., Chang, R. W., Macdonald, A., Shantz, 1605 N., Sjostedt, S., Wiebe, H., and Leitch, W.: Measurements of VOCs by proton transfer reaction mass spectrometry at a rural Ontario site: Sources and correlation to aerosol composition, *Journal of Geophysical Research: Atmospheres*, 114, 2009.
- Wang, H., Wang, J., and Wang, G.: Combination evaluation method of fuzzy c-mean clustering validity based on hybrid weighted strategy, *IEEE Access*, 9, 27239-27261, 2021.
- 1610 Wennberg, P. O., Bates, K. H., Crounse, J. D., Dodson, L. G., McVay, R. C., Mertens, L. A., Nguyen, T. B., Praske, E., Schwantes, R. H., and Smarte, M. D.: Gas-phase reactions of isoprene and its major oxidation products, *Chemical reviews*, 118, 3337-3390, 2018.
- Wold, S., Esbensen, K., and Geladi, P.: Principal component analysis, *Chemometrics and intelligent laboratory systems*, 2, 37-52, 1987.

- 1615 Wu, K.-L.: Analysis of parameter selections for fuzzy c-means, *Pattern Recognition*, 45, 407-415, 2012.
- Wu, R., Vereecken, L., Tsiligiannis, E., Kang, S., Albrecht, S. R., Hantschke, L., Zhao, D., Novelli, A., Fuchs, H., Tillmann, R., Hohaus, T., Carlsson, P. T. M., Shenolikar, J., Bernard, F., Crowley, J. N., Fry, J. L., Brownwood, B., Thornton, J. A., Brown, S. S.,
- 1620 Kiendler-Scharr, A., Wahner, A., Hallquist, M., and Mentel, T. F.: Molecular composition and volatility of multi-generation products formed from isoprene oxidation by nitrate radical, *Atmospheric Chemistry and Physics*, 21, 10799-10824, 10.5194/acp-21-10799-2021, 2021.
- Wyche, K., Monks, P. S., Smallbone, K., Hamilton, J., Alfarra, M., Rickard, A., McFiggans, G. B., Jenkin, M., Bloss, W., and Ryan, A. C.: Mapping gas-phase organic reactivity and concomitant secondary organic aerosol formation: chemometric dimension reduction techniques for the deconvolution of complex atmospheric data sets, *Atmospheric Chemistry and Physics*, 15, 8077-8100, 2015.
- 1630 [Xie, M., Lu, X., Ding, F., Cui, W., Zhang, Y., and Feng, W.: Evaluating the influence of constant source profile presumption on PMF analysis of PM_{2.5} by comparing long- and short-term hourly observation-based modeling, *Environmental Pollution*, 314, 120273, 2022.](#)
- Xie, X. L. and Beni, G.: A validity measure for fuzzy clustering, *IEEE Transactions on Pattern Analysis & Machine Intelligence*, 13, 841-847, 1991.
- 1635 [Xu, Z., Nie, W., Liu, Y., Sun, P., Huang, D., Yan, C., Krechmer, J., Ye, P., Xu, Z., and Qi, X.: Multifunctional products of isoprene oxidation in polluted atmosphere and their contribution to SOA, *Geophysical Research Letters*, 48, e2020GL089276, 2021.](#)
- Yan, C., Nie, W., Äijälä, M., Rissanen, M. P., Canagaratna, M. R., Massoli, P., Junninen, H., Jokinen, T., Sarnela, N., Häme, S. A. K., Schobesberger, S., Canonaco, F., Yao, L., Prévôt, A. S. H., Petäjä, T., Kulmala, M., Sipilä, M., Worsnop, D. R., and Ehn, M.: Source characterization of highly oxidized multifunctional compounds in a boreal forest environment using positive matrix factorization, *Atmospheric Chemistry and Physics*, 16, 12715-12731, 10.5194/acp-16-12715-2016, 2016.
- 1640
- Yang, M. S., Convergence Properties of the Generalized Fuzzy C-Means Clustering Algorithms. *Comput Math Appl* 1993, 25 (12), 3-11.
- 1645
- Yu, J., Cheng, Q., and Huang, H.: Analysis of the weighting exponent in the FCM, *IEEE Transactions on Systems, Man, and Cybernetics, Part B (Cybernetics)*, 34, 634-639, 2004.

- Yuan, B., Shao, M., De Gouw, J., Parrish, D. D., Lu, S., Wang, M., Zeng, L., Zhang, Q., Song, Y., and Zhang, J.: Volatile organic compounds (VOCs) in urban air: How chemistry affects the interpretation of positive matrix factorization (PMF) analysis, *Journal of Geophysical Research: Atmospheres*, 117, 2012.
- 1650
- Zadeh, L. A.: Fuzzy sets, *Information and control*, 8, 338-353, 1965.
- Zaytsev, A., Koss, A. R., Breitenlechner, M., Krechmer, J. E., Nihill, K. J., Lim, C. Y., Rowe, J. C., Cox, J. L., Moss, J., Roscioli, J. R., Canagaratna, M. R., Worsnop, D. R., Kroll, J. H., and Keutsch, F. N.: Mechanistic Study of Formation of Ring-retaining and Ring-opening Products from Oxidation of Aromatic Compounds under Urban Atmospheric Conditions, *Atmospheric Chemistry and Physics Discussions*, 1-24, 10.5194/acp-2019-666, 2019.
- 1655
- Zhang, Q., Alfarra, M. R., Worsnop, D. R., Allan, J. D., Coe, H., Canagaratna, M. R., and Jimenez, J. L.: Deconvolution and quantification of hydrocarbon-like and oxygenated organic aerosols based on aerosol mass spectrometry, *Environmental science & technology*, 39, 4938-4952, 2005.
- 1660
- Zhang, Q., Jimenez, J. L., Canagaratna, M. R., Ulbrich, I. M., Ng, N. L., Worsnop, D. R., and Sun, Y.: Understanding atmospheric organic aerosols via factor analysis of aerosol mass spectrometry: a review, *Analytical and bioanalytical chemistry*, 401, 3045-3067, 2011.
- 1665
- Zhang, Q., Jimenez, J. L., Canagaratna, M., Allan, J., Coe, H., Ulbrich, I., Alfarra, M., Takami, A., Middlebrook, A., and Sun, Y.: Ubiquity and dominance of oxygenated species in organic aerosols in anthropogenically - influenced Northern Hemisphere midlatitudes, *Geophysical Research Letters*, 34, 2007.
- Zhang, Y., Peräkylä, O., Yan, C., Heikkinen, L., Äijälä, M., Daellenbach, K. R., Zha, Q., Riva, M., Garmash, O., Junninen, H., Paatero, P., Worsnop, D., and Ehn, M.: A Novel Approach for Simple Statistical Analysis of High-Resolution Mass Spectra, *Atmospheric Measurement Techniques Discussions*, 1-32, 10.5194/amt-2019-59, 2019.
- 1670
- Zhou, K., Fu, C., and Yang, S.: Fuzziness parameter selection in fuzzy c-means: the perspective of cluster validation, *Science China Information Sciences*, 57, 1-8, 2014.
- 1675
- Zhou, Y. and Zhuang, X.: Kinetic analysis of sequential multistep reactions, *The Journal of Physical Chemistry B*, 111, 13600-13610, 2007.
- Ziemann, P. J. and Atkinson, R.: Kinetics, products, and mechanisms of secondary organic aerosol formation, *Chem Soc Rev*, 41, 6582-6605, 10.1039/c2cs35122f, 2012.